ESTIMATION OF ABOVE GROUND FOREST BIOMASS USING UNMANNED AERIAL VEHICLE IMAGES: A CASE OF ARDHI UNIVERSITY NEIGHBORHOOD

Ezekiel Jilala Shija

MSc. (Geomatics) Dissertation

Ardhi University

May, 2021

ESTIMATION OF ABOVE GROUND FOREST BIOMASS USING UNMANNED AERIAL VEHICLE IMAGES: A CASE OF ARDHI UNIVERSITY NEIGHBORHOOD

By

Ezekiel Jilala Shija

A dissertation Submitted in Partial fulfillment of the requirement for the degree of Master of Science (Geomatics) of Ardhi University

May, 2021

CERTIFICATION

The undersigned do certify that they have read and hereby recommend for acceptance by Ardhi University a dissertation entitled “Estimation of above ground forest biomass using unmanned aerial vehicle images: a case of Ardhi university neighborhood” in fulfillment of the requirement for the degree of Master of Science (Geomatics) of Ardhi University

----

Dr. Dorothea Deus

(Supervisor)

Date----------

Dr. Zakaria Ngereja

(Supervisor)

Date----------

DECLARATION AND COPYRIGHT

I**, Ezekiel Jilala Shija** declare that this dissertation is my own original work and that it has not been presented and it will not be presented to any other university for a similar or any other degree award

Signature……

ACKNOWLEGMENTS

I would, in the foremost, like to thank the Almighty God for the gift of life and embracing all my paths, for without Him I couldn't manage making a way through the unknown territory of despair and extreme situations where the feature entails lay empty and unpredictable every time, I had unusual experience. Every time when I lift up my eyes to the mountains, I realize that the only help that comes without conditions is from God.

Next, I wish to express my sincere thanks to my supervisor, Dr. Dorothea Deus. Her tireless follow-up and comments at each stage of this work has eventually led to its completion in a manner worth of, at least, presenting it to the panel of intellectuals.

May special thanks also go to co-supervisors Dr. Zakaria Ngereja and Dr. Francis Mwakapuja. They always gave constructive comments and instructions that contributed much to this work.

I sincerely acknowledge as well the fruitful work done by Dr. Beatrice Tarimo, Dr. Prosper Ulotu, Professor Martine Hagai and Mr. Mlay. They helped me a lot at different stages of this work.

Thanks also goes to my classmates Mr. Maziku, Ms. Boko and the late Mr. Kakoyo who deserve a special mention here, may he rest in peace. We worked closely together in times of joy and hardships on the course of our studies at the University, may we keep this spirit.

DEDICATION

This work is dedicated to:

My 6 years daughter, Charity E. Shija. She stood as my inspiration throughout my studies at Ardhi University. The end of my studies marks a start of her long way education journey, standard one, though there were coincidental scrambles on scarce family resources to finance our studies. And in extreme situations, I had to pause some stages of this work to let her just started studies go.

The late Kevin E, Shija, my lovely son who passed away on September 4th, 2012. Kevin's eternal parting from us was the greatest blow in our family, which took us off balance and casted a hole before our feature. We rendered all to Jesus who let this happen at the very time we dearly enjoyed and needed his presence. The deep shadow casted by the tomb that awaits us all shall not overturn our faith as the Holy one, Jesus, stands next to it, transforming what appears to us as the finality and making life afresh in eternity.

My lovely wife, Rosemary. Her contribution to my studies is remarkable. She grew patient and energetic to handle all family affairs that needed my attention and did all on my behalf. She always insisted to always kneel before the Lord in prayer and work hard.

My lovely father who passed away when at the final stages of this work, on December 2020. He didn't live to see the peak of my education journey he fully invested his time, moral and financial support since it took off on the first day, he sent me to school. Generally, he will always stand as the effect of whom I am today. May he rest in the hands of Jesus, the Savior.

My lovey mother, whom I have nothing to give in return. She went through different times of joy and hardships for my well-being. May the almighty God reward her all what she deserves

ABSTRACT

Forests provide the biggest carbon pool used to counter-balance the concentration of Green House Gases (GHG) in the atmosphere. Threats of excessive concentration of GHG to climate patterns has drawn much attention around the world that different measures have been taken. Knowledge of the amount of Carbon sequestered by forests is important for appropriate mitigation measures, to this end, various methods are employed for quantification of above ground biomass (AGB). Field techniques yields accurate results but tedious, time consuming and sometimes unsafe for workers. Light Detection and Ranging (LiDAR) and Radio Detection and Ranging (RADAR) are appropriate techniques but involves high costs and complexity in data processing. AGB estimation based on Unmanned Aerial Vehicle (UAV) images is the simple and cost-effective technique suited for small and medium size forests.

In the current study, AGB were estimated using UAV images and compared to AGB estimated based on field observations. The mean AGB estimated from field data was 0.576 t/ha, 0.622 t/ha, and 0.309 t/ha compared to 0.613 t/ha, 0.546 t/ha and 0.245 t/ha estimated using UAV images in sample plot1, sample plot2 and sample plot3 respectively. Likewise, the Root Mean Square Error (RMSE) computed for sample plot1 was 0.087 t/ha while for sample plot2 the RMSE was 0.015 t/ha and for sample plot3 RMSE was 0.516 t/ha. The results suggest the application of the method for small and medium size forests and is recommended down to local government authorities and individual companies in Tanzania to collect forest information that helps combat excessive GHG by taking appropriate measures to prevent much threats.

Key words; Forests; Greenhouse gas mitigation; Above ground biomass estimation methods

Table of Contents

LIST OF FIGURES

LIST OF TABLES

LIST OF APPENDICES

LIST OF ACRONYMS

AGB	Above Ground Biomass
CD	Crown Diameter
CHM	Canopy Height Model
DBH	Diameter at Breast Height
DEM	Digital Elevation Model
DSM	Digital Surface Model
ExGI	Excess Green Index
GCP	Ground Control Point
GHG	Green House Gas
InSAR	Interferometric Synthetic Aperture Radar
LIDAR	Light detection and Ranging
NDVI	Normalized Vegetation Index
NOAA	National Oceanic and Atmospheric Administration
RADAR	Radio Detection and Ranging
REDD+	Reducing Emission from Deforestation and forest Degradation
RGB	Red, Green, Blue
SAR	Synthetic Aperture Radar
SfM	Structure from Motion
TANDEM	Terra SAR Digital Elevation Model
UAV	Unmanned Aerial Vehicle
UNFCCC	United Nations Framework Convention on Climate Change
URT	United Republic of Tanzania
WGS	World Geodetic System

CHAPTER ONE

INTRODUCTION

1.1 Background

The world is experiencing abnormal climate patterns that are attributed to various factors, one being excessive toxic gases emissions into the atmosphere through human activities (González-Jaramillo et al., 2018); Munishi, Mhagama, Muheto, and Andrew (2008). Various factors are attributed to the increase in Green House Gas (GHG) emission to the atmosphere, among which human activities contribute to over 75% through burning of fossil fuel by industries, fuel energy dependent machinery, and forest degradation (Stuart and Pedro, 1998). Large cities and towns are the centers of fossil fuel combustion through industries, cars, and other machines whose main source of energy is fuel. Such extra ordinary injection of carbon dioxide into the air leaves the atmosphere overwhelmed resulting in abnormal trends in climate (Vashum, 2012). To restore the situation and probably prevent much harm in the future, several initiatives and policies have been enacted for implementation at global scale, country level and individual groups. Forests stands as effective means to mitigate global warming and climate change on the earth's surface as they form the largest pool onto which carbon sequestration takes place on the terrestrial ecosystem. Other terrestrial pools that stores carbon are soil organic matter and deed woods (Vashum, 2012). Carbon as one of the Greenhouse gasses stored by plants, absorbs solar radiation and is maintained by natural balance. When this balance is triggered, concentration of Carbon in the atmosphere increases making the earth's surface warmer and upheavals in the global climate patterns may be experienced with associated catastrophes (Jelle G, Bart, Eickhout., Rob, & Rik, 2008). Various mitigation measures have been taken whose levels are determined by quantification of the amount of carbon emitted (Vashum, 2012). Carbon can be estimated in the three pools namely aboveground, belowground and deadwood (Mauya, Mugasha, Njana, Zahabu, & Malimbwi, 2019). The amount of carbon sequestered by forests is quantified through estimation of Above Ground Biomass (AGB) and the quantification may easily be done by employing remote sensing techniques (Shi & Liu, 2017).

AGB estimation is not only useful for quantification of carbon stored by forests but has, as well, got extra ordinary importance in forest inventory, it gives multipurpose ecological indicator useful for distinguishing different plants and animal habitats (Li, Gu, Pang, Chen, & Liu, 2018) it is also

considered as an indicator of ecological processes that gives information on species dominance over an area, hydrology, nutrient cycle, energy capture, information on suitable areas for wildlife (Hiroyuki et al., 2013).

Quantification of carbon through AGB estimation is further emphasized by the United Nations Framework Convention on Climate Change (UNFCCC), one of the international treaties that was adopted in 1992 and became operational in 1994 with the objective of stabilizing the amount of GHG emissions into the atmosphere and limiting feature impacts on climate caused by anthropogenic injection that disturbs the climate systems. Treaties and agreements like the Kyoto Protocol and Paris Agreement, were enacted to enhance the efforts to combat excessive GHG emissions to the atmosphere through burning of fossil fuel (Oppenheimer & Petsonk, 2005). The Kyoto agreement targets on quantitative reduction in GHG emissions and emphasizes more on reduction by forest plantations and management of existing ones and the quantification of reduced emissions is achieved through estimation of AGB (Jelle G et al., 2008). Challenges has, nevertheless, been arising due to conflict of interest between the participants. Industrialized countries are worried of the opportunity cost they should incur as reducing emission would imply reducing industrial productions, and mitigation by forest stands at the expense of settlements and agricultural expansion. These conflict of interests has resulted into variable scales of countries readiness to participate in reduction of their GHG emissions (Cerbu, Swallow, & Thompson, 2011). An incentive-based policy, Reducing Emission from Deforestation and forest Degradation (REDD+), was formulated with the aim of compensating the opportunity cost incurred by countries, companies and individual organizations as a result of stopping using forest products for social and economic purposes. Araya and Hofstad (2016) points out that REDD+ stands as the simple and cost effective GHG emission mitigation measure that is intended to protect much of the forest areas conversion to cropland and source of industrial raw materials and yet pain free for those exercising the forgone benefits from the forests.

The available forest resources in Tanzania can be used to fix problems caused by toxic gases emitted in the atmosphere. Forest covers approximately 48.1 million hectors of the main land, as per Global Forest Resource Assessment (Mugasha et al., 2012a). The forest cover is composed of Miombo woodlands which accounts for 93% of the total forest area (URT, 2017) and are found in the West, South and Central parts of the country. Acacia woodlands are found in the Northern regions, Mangrove forests along the shores of Indian ocean and the closed canopy forest along

Lake Tanganyika. Forests inhabits the natural ecosystem that in turn forms the national social and economic wealth. They are the habitat of wild animals from which the country earns income through tourism, further more forests are source of wetlands and have got a direct influence on weather as they influence water vapor content in the atmosphere which leads to ground precipitation (Zarnoch et al., 2004). Forest degradation through human economic activities has not only being affecting the forest ecosystem, but the climate patterns as well.

Tanzania is one of the countries that agreed to participate in the international treaties to mitigate climate change. Its preparation for participation in the UNFCCC started in 2008 and all issues related to environment and carbon emission reduction strategies were vested for monitoring in the Vice president's office and has so far performed several activities as its readiness for Reducing Emission from Deforestation and forest Degradation (REDD+); (1) Preparation of the national framework for REDD+, (2) action plan and strategy preparation for REDD+, (3) execution of nine REDD+ pilot projects (4) education and awareness to stakeholders (URT, 2017).

As the participating countries in the carbon reduction treaties are obliged to reporting the level of carbon emissions to UNFCCC, several methods that are employed in quantification of carbon sequestered by forests exists through estimation of AGB which can be converted to carbon stock (Schlund & Davidson, 2018). Direct measurements made on site through convention survey techniques are the most accurate of all (Vashum, 2012), but the method is labor intensive, tedious, time consuming and therefore not practical for large area estimations (Yavaşli, 2012). RADAR and LiDAR are remote sensing techniques capable of penetrating below forest canopies and give accurate terrain information covering small to large areas are normally used though they have common problems of complex data processing and huge cost involvement in their operation (Sinha, Jeganathan, Sharma, & Nathawat, 2015). Images from Optical remote sensing sensors can be used to estimate AGB over large areas but the images have coarse spatial resolution that AGB estimation at a tree and stand level is not possible. To date, there are few studies that full address AGB estimation in urban forests, this study therefore attempts to present a simple and cost-effective technique employing images acquired using a small Unmanned Aerial Vehicle (UAV) for AGB estimation of small and medium size urban forests.

1.2 Description of the Study area

The study was conducted at Ardhi University neighborhood located at Ubungo ward, Ubungo district in Dar es Salaam region. The region is located at the shores of Indian ocean in Tanzania between 6º 36´ and 7º 12´ south of Equator and 39º 1´ and 39º 27´ East of Greenwich Meridian as presented in Figure 1.1.

Dar es Salaam is the largest city in Tanzania with the highest rate of fuel combustion from industries and cars and hosts the largest population whose main source of energy and construction material are the forest products. These social and economic needs have got impacts to the balance of carbon concentration in the atmosphere and therefore mitigation by forest plantations should be practiced. The study area was therefore chosen in an attempt to quantify the amount of AGB which leads to the computation of the amount of carbon trapped into these urban forests.

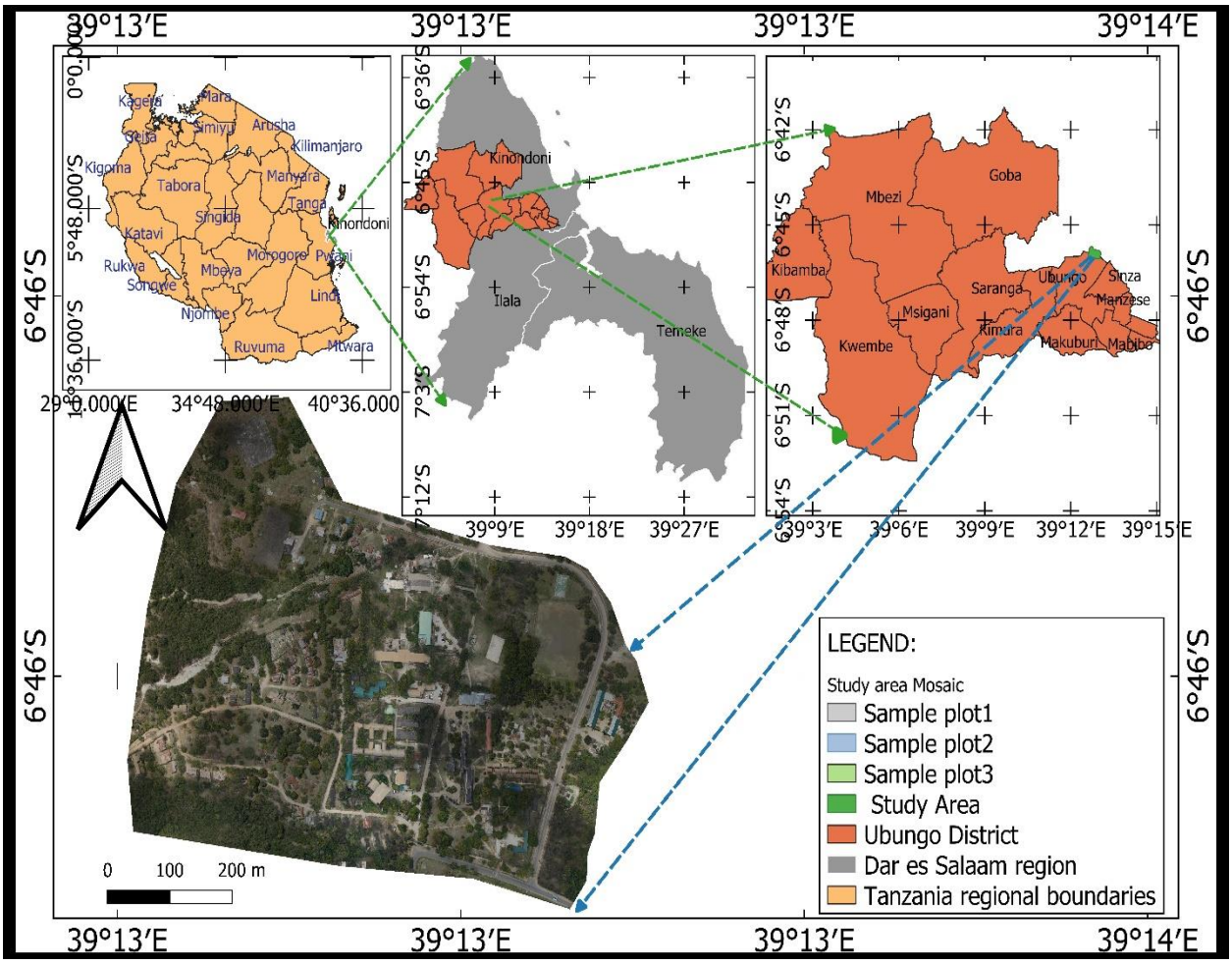

Figure 1.1: Location of the study area

1.3 Statement of the Problem

Deforestation and excessive emission of Green House Gases (GHGs) due to increasing population and industrial activities has been posing threats to the global climate and the natural balance of GHG concentration in the atmosphere. This alarming trend has awakened mitigation measures across nations that includes treaties, policies and agreements all with the aim of reverting the situation back to normal. Tanzania signed an agreement to participate in reduction of Carbon Emissions from deforestation and forest degradation (REDD+) under the United Nations Framework Convention on Climate Change (UNFCCC) which became operational since 2012 (Burgess et al., 2010). One of the most important measures to meet the UNFCC requirements on reducing Carbon and Green House gas emission to the atmosphere is to use simple and cost-effective methods of measuring and updating information on forest Above Ground Biomass (AGB) such measurements subsequently leads to the determination of the amount of emissions (Puliti et al., 2017).

Small and medium size forest plantations can be grown and maintained in cities and towns to fix the alarming rate of fossil fuel injection into the atmosphere and therefore restore the balanced carbon cycle. The amount of fossil injections in form of carbon dioxide gas trapped in by forests can be known through measurement of forest AGB, (Li et al., 2018). This biophysical parameter has been estimated using a number of approaches that differs significantly in terms of complexity in data acquisition, processing, and the associated costs. Images acquired through optical remote sensing for instance, had been extensively used for AGB estimation for decades, with Landsat TM being the primary data source normally free of charge. However, data saturation especially in complex forest structures and poor spatial resolution hinders application of such approach (Lu, Chen, Wang, Moran, Batistella, Zhang, Laurin, et al., 2012). LiDAR and RADAR are remote sensing approaches widely used to estimate AGB with common unique capability of penetrating forest canopies town to the terrain enabling computation of tree heights as the parameter useful for AGB estimation. However, they have common hindrances of complex data processing and huge costs involved in data acquisition (Sinha et al., 2015; Vazirabad & Karslioglu, 2011). Urban forest is the rare studied type of forest in Tanzania and owing to this, less is said about its contribution to fixing the concentration of toxic gases in the atmosphere nor about the appropriate AGB estimation method. This study presents a simple and low-cost approach that may be considered as alternative AGB estimation method for small and medium size open canopy forests employing UAV images.

1.4 Main Objectives of the Research

To present a simple and cost-effective approach to estimate AGB for small and medium size Urban forests in Tanzania using UAV images.

1.5 Specific objectives of the Research

In order to carry out this study, three specific objectives were identified:

a) To carry out ground Forest inventory and from the data estimate forest AGB
b) To process UAV images and then estimate forest AGB
c) To validate the AGB estimated Using UAV images.

1.6 Research questions

The findings of this study highlight appropriate answers to the following key questions

a) How well can the DBH and tree height derived from UAV images predict AGB?
b) Can UAV imageries be reliable and alternative data source for small and medium size forest AGB estimation?

1.7 Dissertation organization overview

This work is organized in five chapters where chapter one gives an introduction of the research and highlights the research problem. Chapter two gives an overview of the existing research works on the subject matter and gives detailed explanations of the methods commonly used for AGB estimation, data processing techniques and gives an in-depth classification of UAV platforms. Chapter three explains the methods employed in the study where data acquisition and processing techniques are explained in detail. Chapter four presents the results of the methods employed with the corresponding discussion and the final chapter gives the conclusion and recommendations based on the key findings of the study.

CHAPTER TWO

LITURATURE REVIEW

2.1 Above Ground Biomass Overview

The amount of carbon stored in plants is quantified through biomass estimations (Schlund & Davidson, 2018) and forests constitutes the largest terrestrial pool onto which carbon is trapped (Salunkhe, Khare, Kumari, & Khan, 2018). This pool has been hit by threats posed by human beings that the world is today witnessing abnormal trends in Green House Gas (GHG) emissions to the atmosphere attributed to technological inversions like industries and locomotives that inject excessive amount GHG in the atmosphere these emissions disturbs the natural balance of carbon leading to, among other things, unusual trends on climate (Figure 2.1) (Jelle G et al., 2008). Up-to-date and accurate estimation of AGB is therefore important to quantify the mitigation measures as a requirement of the United Nations Framework Convention on Climate Change (UNFCCC) (Temesgen, Affleck, Poudel, Gray, & Sessions, 2015)

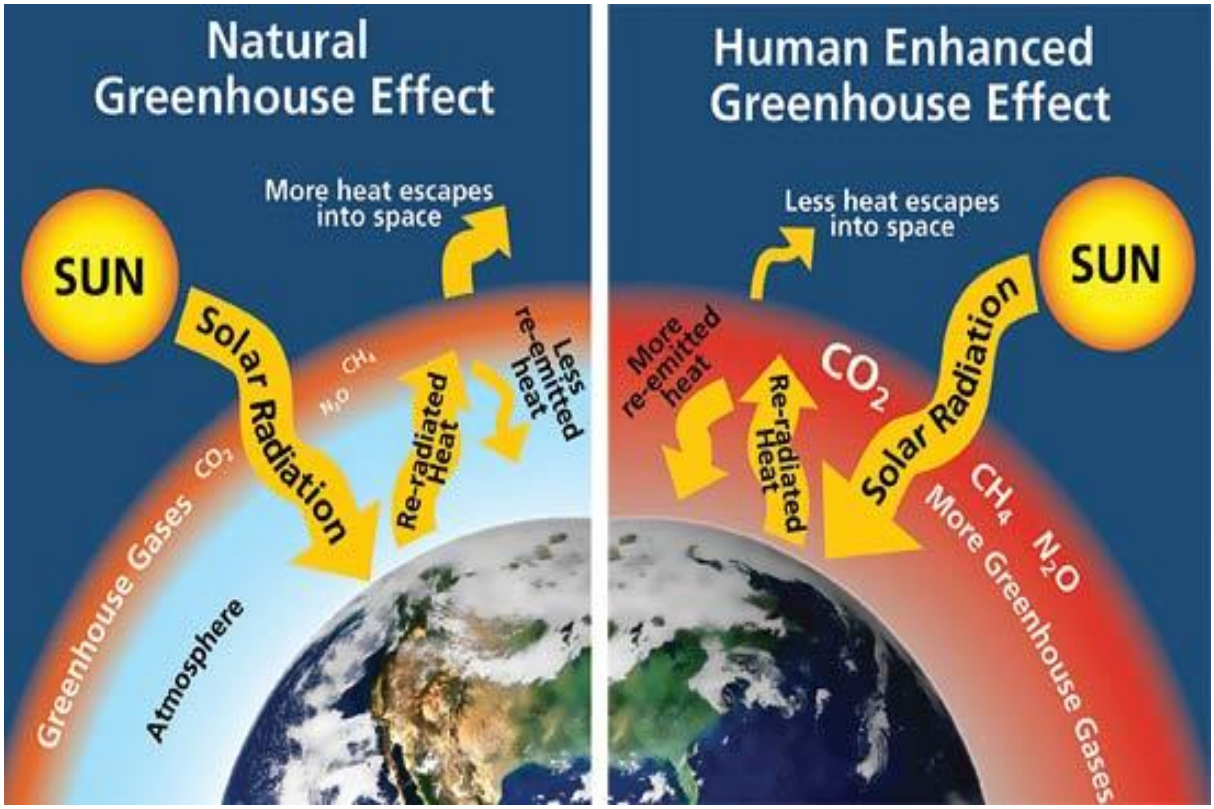

Figure 2.1: The effect of GHG emission into the atmosphere (Source: Centre for Climate and Energy Solutions-www.c2es.org)

2.2 Above Ground Biomass studies

Quite a number of studies has been undertaken related to forest biomass around the world in an attempt to quantity the amount of carbon sequestered by the forests. This is attributed to the fact that concentration of carbon dioxide in the atmosphere accounts for over 60% of the causes of global warming and climate change (Vashum, 2012).

Sileshi (2014) analyzed the challenges of choosing a proper allometric model to apply when estimating AGB after collection of the required sample data for a particular study. The choice of allometric model to use becomes a challenge when more than one model exists over a particular species or vegetation type. The study mentioned three stages to which AGB estimation has to go through namely individual tree level AGB estimation, plot level AGB estimation and the mean values across plots for forest level AGB estimation. Important forest parameters estimation influences the final estimated AGB and so the choice of an appropriate model, from existing ones is the matter of great concern to reduce artifacts in the final estimation. The study then analyzed different published allometric models and lacking clarifications on the involved parameters and suggested ways for users to get informed on the merits and reliabilities of the models they intend to apply for AGB estimation.

Macedo et al. (2018) estimated AGB in South Portugal using Normalized Difference Vegetation Indices derived from high resolution satellite images. Their study aimed at developing a model that would be used for biomass estimation for other regions. The model best estimated AGB and was recommended for use in similar regions.

Puliti et al. (2017) modelled AGB in Miombo woodlands of Southern Tanzania using TANDEM-X data. The primary objective of this study was to establish a model that links AGB with Interferometric Synthetic Aperture Radar (InSAR) heights from World-DEM. Circular sample plots were designed for collecting field data for which Diameter at Breast Height (DBH) of all trees in each sample plot were measured, and sample tree heights measured, AGB was then estimated with DBH and tree heights as inputs in the model. The study revealed that InSAR data are well suited for large area AGB estimation in Tropical woodlands. Despite the promising results, InSAR

heights requires normalization from either field sampled data or Lidar data making the process time consuming and costly.

Lu, Chen, Wang, Moran, Batistella, Zhang, Vaglio Laurin, et al. (2012) gave an overview of integrating Landsat with Lidar data to overcome the saturation problem encountered with Landsat data when are used to estimate AGB. In this study Landsat Thematic Mapper data were used to estimate AGB of the Amazon forests in Brazil. Spectral signatures and textures information derived from the TM image led to good estimates of AGB. The main shortcoming found with this approach was saturation when biomass density exceeded 150 T/ha. This was due to insensitivity of spectral signatures as forest structures became more complex. Integrating Lidar data sets overcame saturation problem. It was concluded that AGB estimation using Landsat data is only suitable for areas with relatively simple forest structure.

Deng, Katoh, Guan, Yin, and Li (2014) assessed the potentials of integrating World View 2 data with L-Band Synthetic Aperture Radar data to Estimate AGB at Purple Mountain national Park in China. The L-Band datasets, in dual polarization mode (HH and HV), were used to derive features relationships from scattering information and the generated NDVI maps from Landsat images were resample to 10m spatial resolution to match with backscatter maps. The Combined Volume Index model that incorporated backscattering of polarized and the spectral bands resulted into good AGB estimation.

Mutwiri, Odera, and Kinyanjui (2017) assessed the potentials of LiDAR in estimation of tree height and AGB) in Londian forest, south-western Kenya. Two datasets were collected and used for this study; LiDAR datasets that were acquired from a sensor mounted onto an aircraft that flew at altitude of 1550m. Field collected data from selected sample plots were DBH and tree heights. LiDAR datasets were processed using Lastool where points were classified and the CHM created as the difference between DSM and DTM. Tree height were then extracted from the CHM and DBH Predicted from linear regressions. The field sampled data were used for validation. Results from the study shows high correlation between AGB and tree heights estimated from LiDAR datasets, and AGB and tree height measured from field surveys. Many studies have shown LiDAR to be the perfect approach for acquiring information on the structure of forest resources especially

in complex and dense canopy covers, (González-Jaramillo et al., 2018; Wallace, Lucieer, Malenovský, Turner, & Vopěnka, 2016b), however application of LiDAR is associated with huge operation costs as pointed out by Birdal, Avdan, and Türk (2017).

Iizuka, Yonehara, Itoh, and Kosugi (2017) assessed the potentials of predicting forest parameters, at Kiryu Hydrological Watershed near Otsu City in Japan, from UAV Photogrammetry. The study employed structure from Motion (SfM) algorithm to generate three-dimension models, the DSM and DTM from two-dimension UAV images. CHM was then generated as the difference between DSM and DTM from which forest parameters were extracted. The CHM was segmented to extract tree heights and predict DBH from tree crowns and regression analysis. The study was validated by field sampled data where results shown good correlation between the tested variables. This study and many other studies such as Kachamba, Ørka, Næsset, Eid, and Gobakken (2017), gave highlights of employing the SfM algorithm and UAV photogrammetric techniques to successively and correctly estimate forest AGB

2.3 Forest Above Ground Biomass Estimation Methods

There is quite a number of AGB estimation approaches. Different studies like those discussed on the foregoing section has shown the strengths and weakness of each. Field survey methods yields accurate estimation but at the expense of time, cost and sometimes workers safety, while Optical remote sensing images comes with coarse spatial resolution and so forest parameter estimation at a stand level may not be achieved. Synthetic Aperture Radar (SAR) is suitable for global scale AGB estimation but requires complex data processing and LiDAR is capable of giving accurate forest parameters for AGB estimation but involves huge operating costs that are sometimes not manageable by individual and organization (Tang & Shao, 2015)

AGB estimation methods can therefore be categorized into two main techniques namely field survey where forest inventory is directly done on site and indirect methods where remote sensing data are used to estimate forest parameters which are key inputs in the allometric models or regression equations adopted for AGB estimation (Sileshi, 2014). Sections 2.4 and 2.5 gives detailed explanations of the two main methods used for AGB estimation.

2.4 Field survey techniques

Field survey methods are regarded as the most accurate estimation methods where forest parameters are directly measured on site at selected sample plots (Temesgen et al., 2015). The parameters directly measured on site are DBH, tree height and crown diameter. These parameters can either be measured by destructive techniques where sample trees are fell down then various components are measured accurately. The harvest method is often opted when developing biomass allometric models for use in large scale AGB estimation (Yavaşli, 2012). Non-destructive techniques do not involve cutting down tree, rather parameters are measured and allometric model applied to estimate AGB.

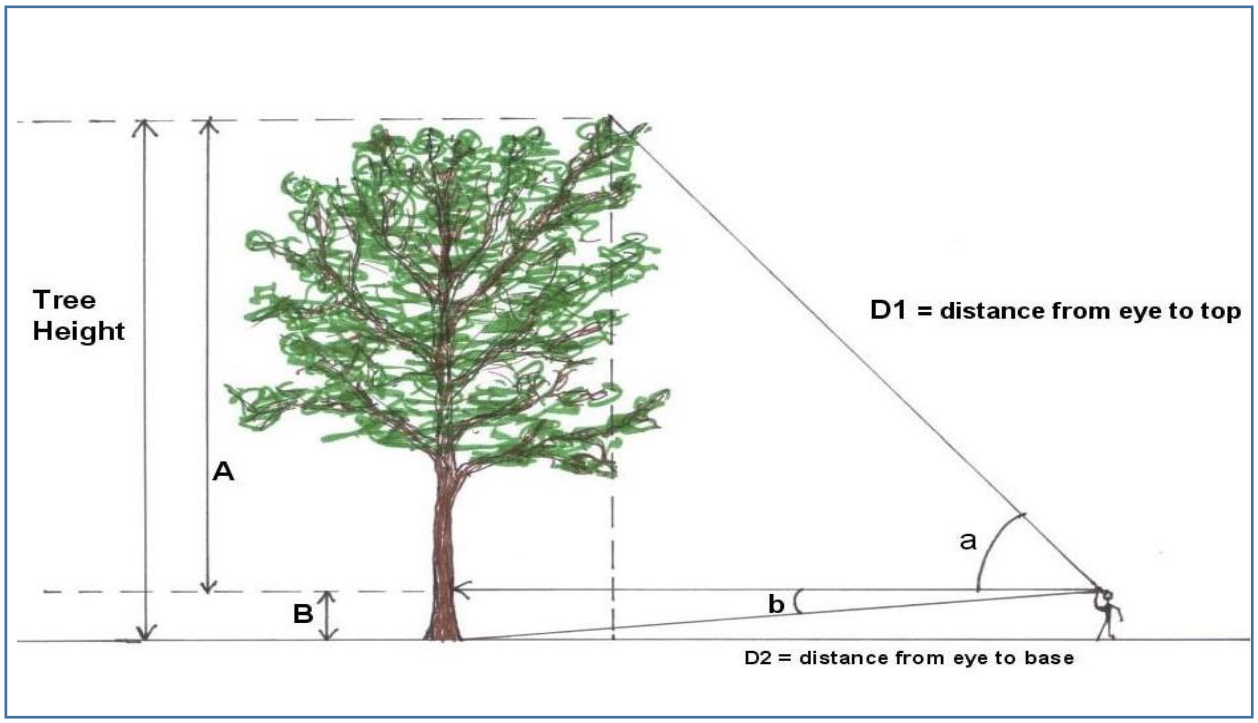

Figure 2.2: Tree height measurement (Blozan, 2006)

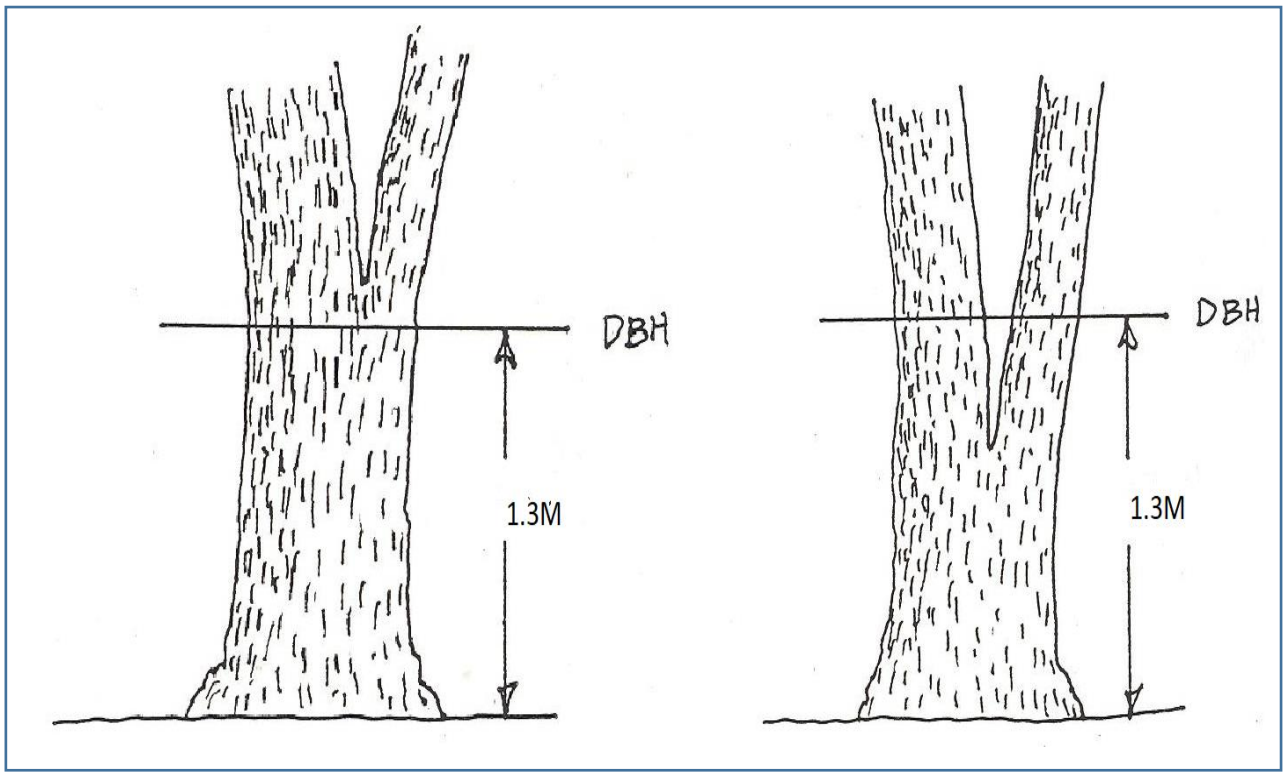

Figure 2.3: Tree DBH Measurement guidelines (Malone, Liang, & Packee, 2009)

Tree heights can be measured in the field by employing different approaches, such as measurement of vertical angles from the instrument line of sight to the top of the tree and horizontal distances from the measuring instrument to the foot of the tree (Figure 2.2) and final deduction of tree heights done by mathematical computations basing on the formulated geometric figures. Total stations and rangefinder are some of the measuring instruments which can used.

Tree DBH measurement is easily done on site and usually at a height of 1.3m from the foot of the tree (Figure 2.3) using a special measuring tape with clippers or a normal tape where circumferences of tree stems are measured and later DBH calculated using mathematical models (Malone et al., 2009). Generally estimating AGB by field survey methods is the time consuming, tedious, costly and may put workers safety at a threat and therefore other methods are preferred instead.

2.5 Remote Sensing Techniques

Remote sensing technology has come with complete revolution on the methods of capturing data for the forest ecosystem. Tedious, destructive and sometimes hazardous field techniques are now

confined to allometric model's development. Massive forest data may now be collected by remote sensing techniques (Holopainen, Vastaranta, & Hyyppä, 2014). With remote sensing techniques, important forest parameters useful for AGB estimation can be estimated to a reasonable accuracy. These techniques can be categorized into two main groups based on the sensor namely active remote sensors and passive sensors. The techniques are discussed in the following sub-sections.

2.5.1 Active Sensors

Active sensors have the capability to generate energy making it possible to capture data day and night and therefore overcoming obstacles encountered with optical remote sensing that depends on the sun's illumination**.**

(i) **Synthetic Aperture Radar (SAR)**

SAR is the remote sensing technique useful for studies on forest structure on the global coverage and estimation of forest above ground biomass. SAR technique has got distinctive features such as penetrating forest canopies, cloud and fog, non-dependence on solar as the source of energy and therefore rendering it as the all-weather, day and night imaging technique (Sinha et al., 2015). The most useful bands for AGB estimation are X and C bands which scatters from the top of forest canopies and so carries much information of tree leaves. Higher frequency L , S and P bands have higher forest canopy penetration capacity and so they facilitate estimation of forest canopy height (Schlund & Davidson, 2018). When two or more SAR images of different phase angles are used, the technique is called Interferometric SAR (Schreyer, Geis, & Lakes, 2016). SAR technology may be looked at as the only technique capable of providing global data for forest structure though it has some constraints that limit its wide applications such as complex data acquisition, processing and associated huge operation costs (Sinha et al., 2015)

(ii) Light Detection and Ranging (LiDAR)

LiDAR is an active remote sensing technique that uses light beams to scan the objects and collects massive points. Pulses of laser are emitted from the scanner mounted on either unmanned aerial vehicle platform, manned aerial vehicles or on a stationary platform. Once the laser pulses hit the objects and basing on the speed of the laser pulse, and the time taken, distances between the scanner and the scanned objects are determined. The speed, time and scan angle, enables computation of

three dimension position of reflected objects basing on the correction signals sent from GNSS receiver and on board Inertial Measurement Unit (Jamie et al., 2012).The beauty of this technology is the capabilities of the laser pulses to penetrate forest canopies, making it a unique technology to capture data for forest resource inventory (Lenda, Uznański, Strach, & Lewińska, 2016).The acquired point data are used to generate DSM and DEM and subsequent data for AGB estimation (NOAA, 2012). Though LiDAR remote sensing stands as an alternatives technique for capturing information on the vertical structure of forests that leads to the most accurate DEM, its associated high costs, data processing complexity creates a barrier on its application for AGB estimation (Birdal et al., 2017).

2.5.2 Passive Sensors

Passive sensors depend on the Solar's energy illumination to capture and record the information reflected from the targets and microwave passive sensors records thermal energy signals emitted by objects.

(i) Optical Satellite Images

Satellite images acquired by passive sensors have been used to estimated AGB for large areas by utilizing spectral reflectance or Vegetation Indices such as Normalized Vegetation Index (NDVI). However, use of optical satellite images alone is faced by data saturation problem, poor spatial resolution and cloudy images that makes AGB estimation at tree and stand level impractical. Following such constraints, other techniques for AGB estimation are preferred (Deng et al., 2014)

(ii) Unmanned Aerial Vehicle (UAV) Photogrammetry

Remote piloted aircrafts have long been in the military use for decades now. In the 1990s these types of aircrafts descended into civilian use and are now in the market for a number of applications including science and research, agricultural monitoring, forest management, monitoring of natural hazards and other applications (Watts, Ambrosia, & Hinkley, 2012). Figure 2.4a-f provides a summary of UAV platform categories as classified by Watts et al. (2012);

a) **Macro Air Vehicle (MAV)**: these are very small platforms normally designed for military applications to carry out short mission profile surveillance in hostile and dangerous scenarios. They are portable by individual soldiers and capable of flying to an altitude less than 330m with battery flight endurance lasting in 30 minutes.

b) **Vertical Take-Off and Landing (VTOL)**: these are the rotary wings platforms that does not require a runway for take-off and landing and therefore suitable for limited open and areas. The platforms are portable with rechargeable batteries that can endure a flight of less than an hour and can fly on variable heights. They are widely applied for small and medium size forest and agricultural studies, rescue operations, capturing data in complex urban settings and many other civilian applications

c) **Low Altitude, Short Endurance (LASE)**: these are small UAV platforms with fixed wings design designed for quick field operations with 1 to 2 hours battery flight endurance.

d) **Low Altitude, Long Endurance (LALE)**: these are upper versions of small UAV platforms with an improved battery endurance and with different civilian applications.

e) **Medium Altitude, Long Endurance (Wallace, Lucieer, Malenovský, Turner, & Vopěnka)**: these are platforms with larger designs than small UAV platforms. They can fly up to an altitude higher than 9000m with the battery that can endure long hours of continuous field operations when the flying altitude is at most 5000m and therefore suitable for large area studies. The platform is mostly utilized for military operations but can as well be used for civilian applications such as wildfire imaging.

f) **High Altitude, Long Endurance (HALE)**: these platforms are the largest and newest of all autopiloted systems and are even bigger than many civilian manned crafts. They can fly to an altitude higher than 20,000m covering extremely larger areas for global scale mapping and military applications but are cost prohibitive for most of the civilian applications. Outside the US military applications, NASA and National Oceanic and Atmospheric Administration (NOAA) employ HALE for global scale data collections for earth and atmospheric investigations.

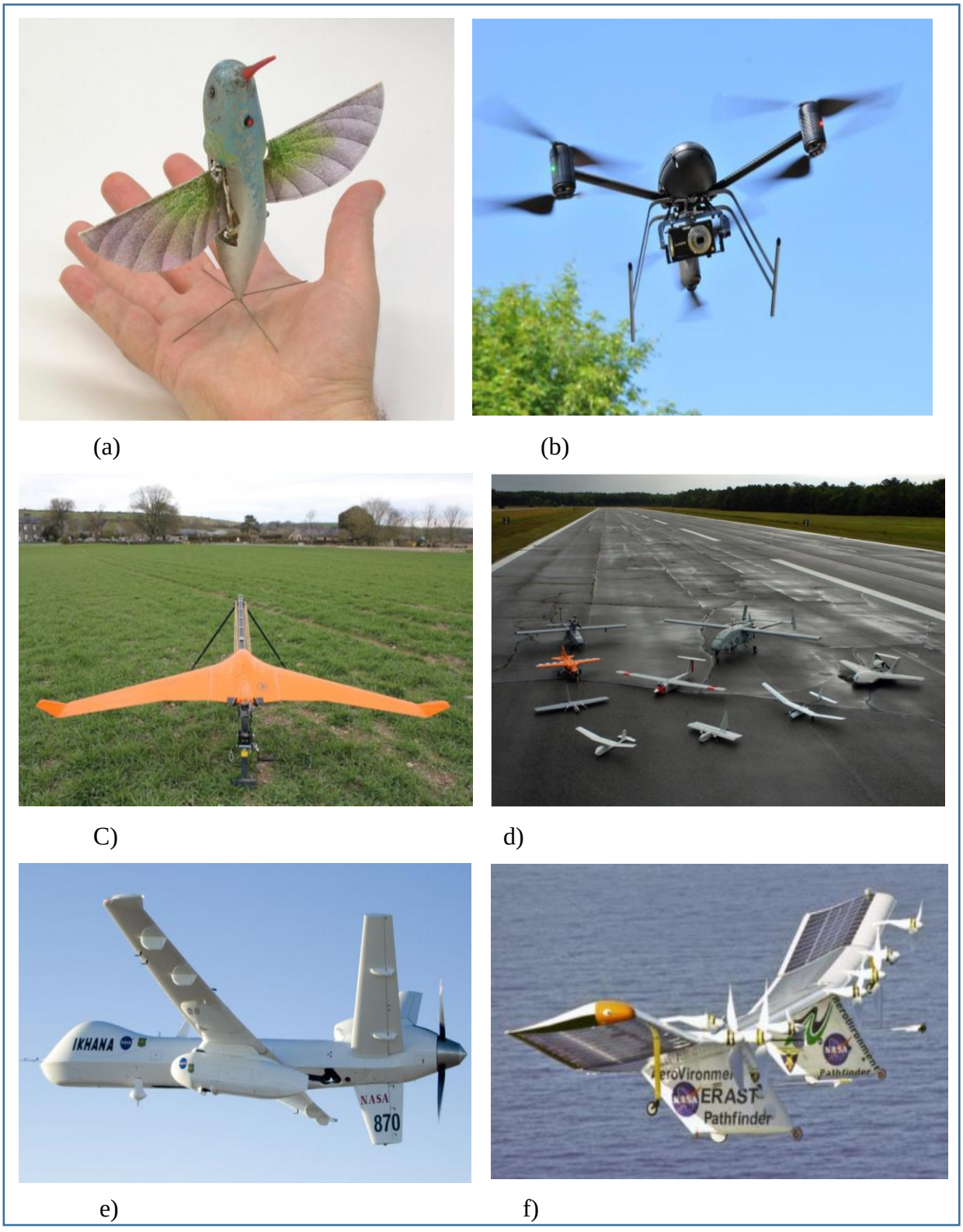

Figure 2.4: Types of UAV platforms - (a) MAV (b) VTOL (c) LASE (d) LALE & MALE (e) MALE (f) HALE (Watts et al., 2012)

UAV has gained wide applications in many scientific disciplines including forest resource management practices. UAV has emerged as the simple, cost effective and alternative method of mapping then deriving forest parameters that enables estimation of forest above ground biomass. With the flight plan done in a computer, the autopilot software controls cameras mounted on the UAV platform to capture a series of overlapping two-dimension images which are later processed using Structure from Motion (SfM) algorithm to reconstruct three-dimension images for Digital Surface Models (DSM) and other derived products useful for estimation of Above Ground Biomass.

Structure from Motion (SfM) with its origin from Computer Vision, is the algorithm that uses the same principles as stereo photogrammetry of reconstruction of three-dimension models from two dimension overlapping images. The only basic difference in that SfM automatically generates the geometry of the scene, camera position and orientation through image bundle adjustment procedure. The reconstructed 3D models are transformed from image space coordinate system to real world system by georeferenced the model using photo Ground Control Points (GCPs) accurately measured by field survey techniques. With the georeferenced 3D model, products like Digital Surface Model (DSM), Digital Terrain Model (DTM) and orthophoto mosaic may be generated (Westoby, Brasington, Glasser, Hambrey, & Reynolds, 2012).

A research conducted by Otero et al. (2018), reveals that UAV photogrammetric techniques performs quite well in a forest with homogeneous species. Due to poor penetration of optical images under the canopies, ground filtering algorithms are used to derive Digital Elevation Models (Özdemir & Remondino).

UAV images are processed using various software packages that utilize SfM algorithm. A study conducted by Murtiyoso, Grussenmeyer, Börlin, Vandermeerschen, and Freville (2018) reports that Agisoft Metashape pro software and its predecessor versions simplifies the photogrammetric workflow and attains accurate processing results. The study, however reported fewer detailed descriptions of how the processing algorithms works. With newer versions processing reports are given and may, at least, be used to trace and identify problems in case of unsatisfactory results.

2.5.3 Image Segmentation

Lim et al. (2015) defined Image segmentation as the partitioning of an image into homogeneous similar disjoints that are non-overlapping. Image pixels with similar values are grouped together to form image objects that can be analyzed in different platforms to give spatial details for different applications. Schiewe. (2002) points out the principles that underlies images segmentation techniques, he highlighted the principles of neighborhood and similarity. Similarity measure compares elements of one object and the other in the immediate neighborhood under a certain threshold and fuses them together to make one object.

Image segmentation has been used for forest studies for tree crown delineation to identify individual trees to simplify tree counting and tree height estimation, classification thence calculation of vegetation indices. The invention of this technique has improved processing of remote sensing images to derive important forest parameters and has made it possible to acquire datasets covering a large area at a considerable short time and less cost when compared to data acquisition by conventional field techniques(Baatz & Schäpe, 2000).

Avola et al. (2019) discussed in detail the possibility to overcome a narrow choice of channels in most of UAV images where there is no Near Infrared (NIR) band. Various indices that does not incorporate NIR channel have been developed and the study points out that they perform even better.

2.6 Allometric Models for AGB estimation in Tanzania

Allometric models are mathematical equations that relates variables which are used for above ground biomass estimation from either field inventory data or remotes sensing data. Allometric models are developed by measuring tree variables mainly by destructive sampling where selected samples trees are fell down and respective variables such diameter at breast height, tree height, and density are measured (Jucker et al., 2017). Allometric models vary with forest species, topography and location, therefore one model may be suitable for certain forest species in one location but may not predict well in the other, for this reason various allometric models are developed for biomass estimation basing on the aforementioned considerations (Malimbwi, Eid, & Chamshama, 2016).

In Tanzania the forest is composed of a diversity of plant species such as dry miombo woodlands, wet miombo woodlands, mangrove forests on the shorelines, montane forest and plantation forests (W.A. Mugasha et al., 2012). Following this, a number of allometric models has therefore been developed to cater for this bio-diversity and finally yield reliable results on biomass estimation. Malimbwi et al. (2016) compiled a list of developed models that covers the diversity of plant species used for biomass estimation in Tanzania as presented in Table 2.1

Table 2.1: Allometric models for AGB estimation in Tanzania (Malimbwi et al., 2016; Munishi et al., 2008)

S/n	Biomass Model	Forest type for application
1	AGB=$0.1027 \times dbh^{2.4798}$ AGB=$0.0763 \times dbh^{2.2047} \times ht^{0.4918}$	Miombo Woodlands
2	AGB = $0.25128 \times dbh^{2.24034}$ AGB=$0.19633 \times dbh^{2.07919} \times ht^{0.29654}$	Lowland and humid Montane
3	AGB= $0.25128 \times dbh^{2.24034}$ AGB=$0.19633 \times dbh^{2.07919} \times ht^{0.29654}$	Mangrove forests
4	AGB= $0.3154 \times dbh^{2.3189}$ AGB= $0.0292 \times dbh^{2.0647} \times ht^{1.0146}$	Acacia Woodlands
5	AGB= $0.0550 \times dbh^{2.5968}$ AGB= $0.0357 \times dbh^{2.4679} \times ht^{0.2809}$	Pine forests
6	AGB= $0.3356 \times dbh^{2.1651}$ AGB= $0.1711 \times dbh^{2.0047} \times ht^{0.3767}$	Plantations(hardwood)
7	AGB = $0.5927 \times DBH^{1.8316}$	Urban forest
9	AGB= $2.234966 \times dbh^{1.43543}$ AGB=$0.192416 \times dbh^{1.204898} \times ht^{1.204898}$	Baobab tree

2.7 Statistical analysis

Statistical analysis is the standard procedure employed in researches to assign meanings to meaningless numbers that helps to draw correct interpretation thence reporting of research findings (Ali & Bhaskar, 2016). It is an important ingredient of a research that is commonly used to analyze the collected or processed data and finally come up with meaningful summaries (Ibrahimi, 2018).

Ali and Bhaskar (2016) categorized methods of analyzing data;

a) **Descriptive statistics**: this type of analysis establishes the relationship between variables of the sample or population by using mean, median and mode and provides a summary that best represents the data where other information such as minimum and maximum values, range, standard deviation and variance can be presented.
b) **Inferential statistics:** this makes use of random samples of the population for analysis whose findings reflects the whole population. It uses statistical tests (t-test) to establish the relationship between variables where the calculated probability with values that ranges between 0 and1 commonly known as the P-value is used as the criteria for comparison of variables.

However, Andrade (2019) highlighted very important cautions regarding the misinterpretations of the statistical testing. As per this study, concluding a research basing on P-Value, the arbitrary threshold set on a continuous random variable, may sometimes lead to false conclusions as P-Value does not, in itself, justify or nullify the findings of the research, rather, other measures of size such as mean values of the samples, the nature of the sample, sample size, reliability of the sample collection method should be considered. In the same context, Gibbons and Pratt (1975) also emphasized that statistical significance or non-significance does not necessarily imply practical significance or non-significance though stands as an objective measure, when other factors are considered, that helps to reach a practical decision making.

CHAPTER THREE

METHODOLOGY

3.1 Overview

The flow of this research consists of the following activities; reviewing the existing literatures on AGB estimation, forest inventory on the selected sample plots, Ground Control Points establishment on the research area, data processing, AGB estimation, statistical analysis and validation of the results. The study integrates GIS, remote sensing and photogrammetric techniques to estimate forest AGB using UAV images taken in an off- leaf season covering the three selected sample plots, and the overall study area. The images were pre-processed and processed using Agisoft Metashape Professional, QGIS and some were performed in ArcGIS. Results were validated by comparing AGB estimated based on UAV images with that estimated based on field inventory data.

Field data were collected on the selected sample plots using a tape measure for DBH measurements and a total station that was used to collect data for tree height and sample plot positions. Field data were later processed and AGB computed using appropriate allometric models given in Table 2.1. The flow of the methods employed in this study from data acquisition to validation of the results is presented on Figure 3.1.

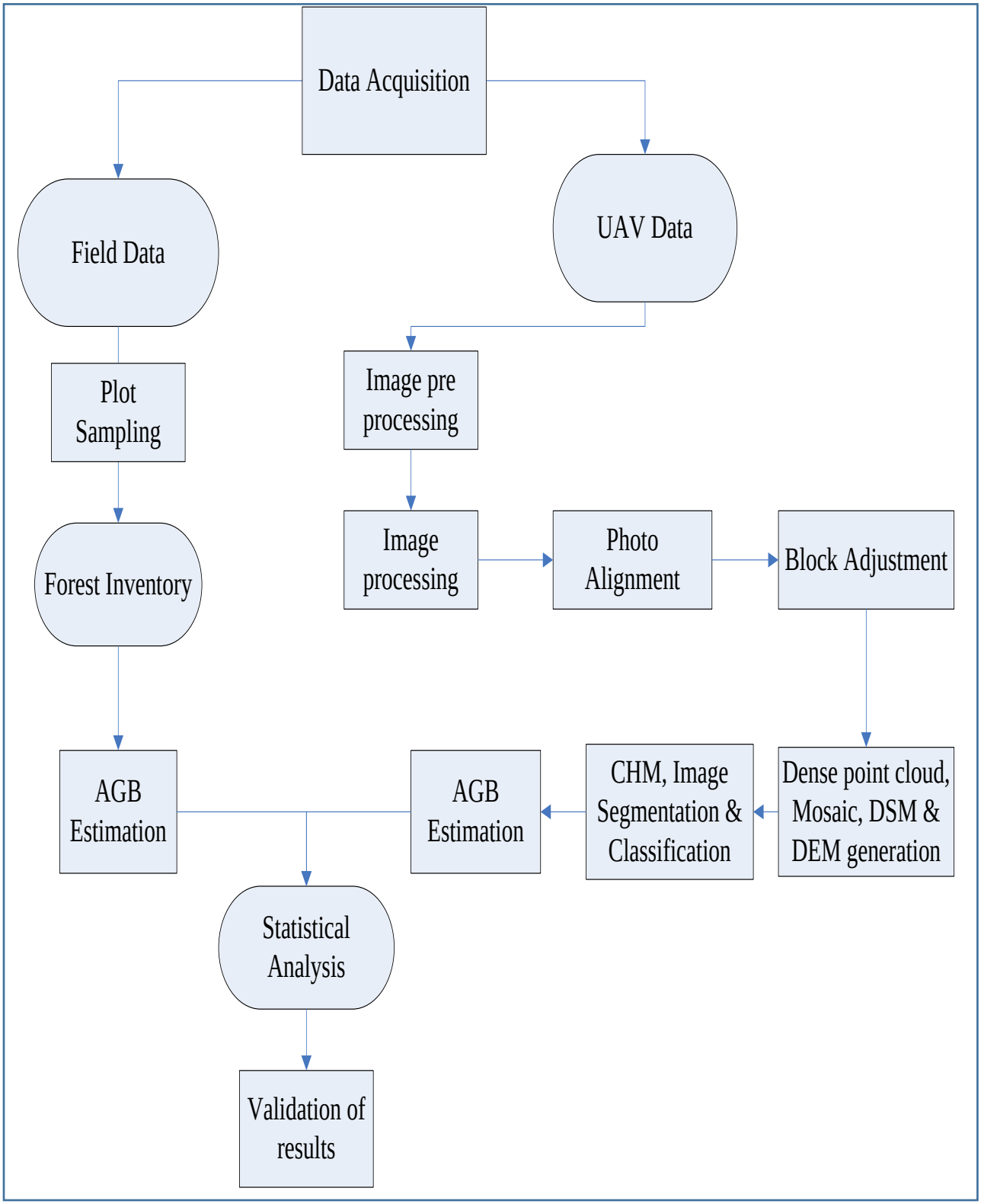

Figure 3.1: Methodology flow chart

3.2 Instrument and software used

Various instruments/tools and software were employed at various stages of the study as listed in the table 3.1.

Table 3.1: Equipment and software used

S/N	**Software**		**Instrument/Tool**	
	Name	Use	Name	Use
1	Excel	Data processing and Statistical analysis	Tape measure	Forest Inventory
3	Agisoft Metashape Professional	UAV image Processing	Data sheets	Recording of forest inventory data
4			Leica TS 9 Total Station	Photo control extension, sample plot location & tree height measurements
5	QGIS 3.8	Image Processing		

3.3 Data Collection

This section describes the data and the methods employed on the data collection process. Forest field inventory data and UAV images were used for this study. The field inventory data consisted of tree stem perimeters, vertical angles, sample plots corner coordinates and horizontal distances and the UAV images covering the study area.

3.3.1 UAV Images

The UAV images utilized were acquired in September 2018 using a fixed wing light weight UAV flying at an altitude of 409m above the ground, resulting into 829 images with Ground Sample Distance (GSD) of 4.8cm. A pose file that describes camera positions and orientation for image alignment and block adjustment was provided together with the images.

3.3.2 Ground Control Points establishment

Ground Control Points (GCPs) were established to enhance the accuracy of the models and the resulting point cloud. According to a study conducted by Oniga, Breaban, and Statescu (2018) at least three GCPs are required to enhance accuracy of the three dimension information derived from UAV products. It was further revealed that GCPs have higher influence on the quality and accuracy 3D products generated from the images and therefore the higher the number of GCPs used for georeferencing the higher the resulting accuracy.

Using the existing unprocessed UAV photographs, appropriate points which clearly appeared in the photographs were chosen and reconnaissance done on site to identify the selected points to be used as GCPs. The points were chosen with a criteria of meeting good coverage of the study area (Figure 3.2) In this study twelve control points and four check points were identified in the photographs as well as on the ground. These were coordinated using a high precision Leica TS 09 total station basing on a network of existing control point around Ardhi University neighborhood in WGS 84 coordinate system. The existing control had no elevation above mean sea level, and therefore differential levelling using SOKKIA BM 40 automatic level was undertaken to induce the control points with elevation above mean sea level from a known benchmark.

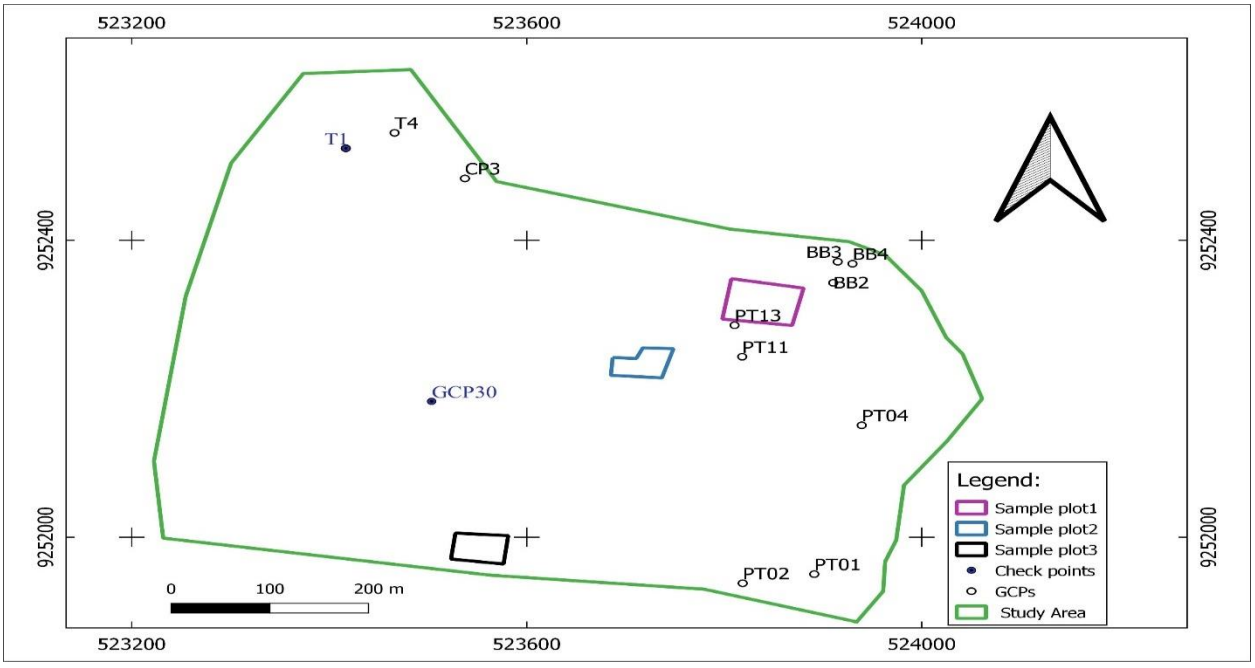

Figure 3.2: GCPs and Check Points distribution over the study area

3.3.3 Forest field Inventory

The study area consists of planted trees where three 75m by 35m, 51m by 41m and 58m by 38m rectangular like sample plots were selected. The position of each plot was measured using the Leica TS 09 Total station (Figure 3.4). In each plot ten trees were selected randomly as done by Otero et al. (2018) and Kachamba et al. (2016) for heights measurements. The total station was then used to measure distances of each from the instrument setup and angle of inclination from the reflector prism positioned on the foot of each tree (Blozan, 2006) as shown in diagram presented in Figure 3.3.

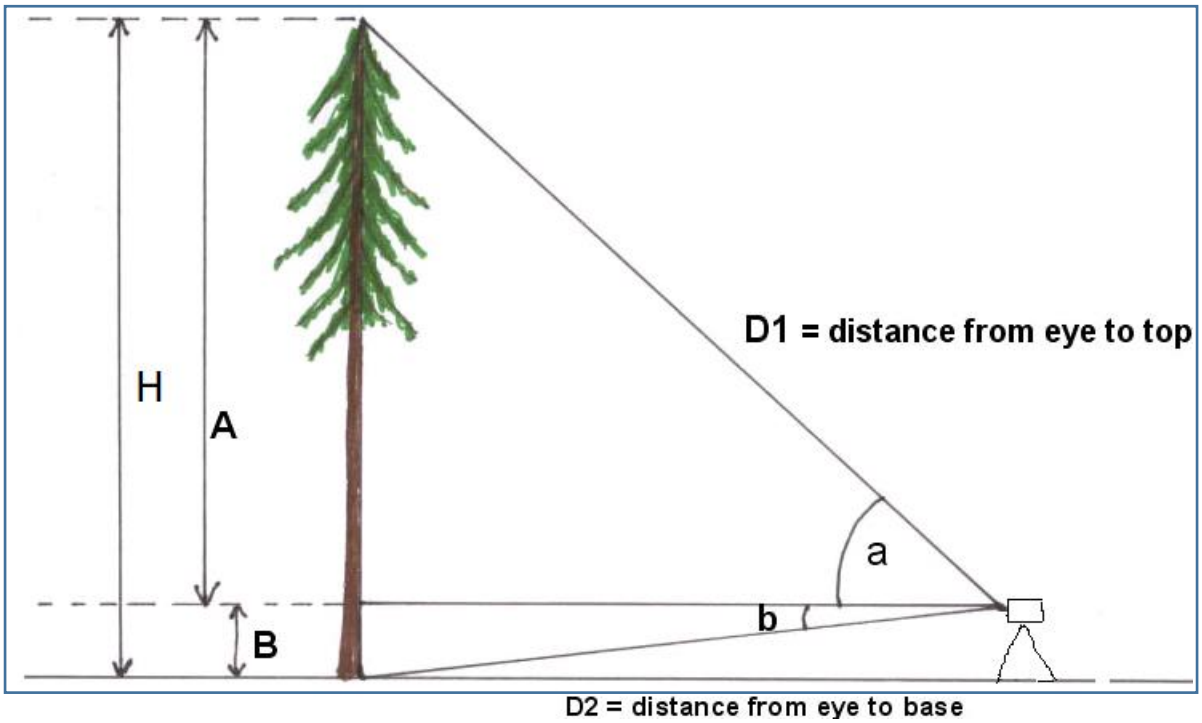

Figure 3.3: Tree height measurement procedures (Blozan, 2006)

From the diagram, the angle of inclination 'a' and the horizontal distance 'D2' were measured onsite and equations 3.1 and 3.2 were used to compute the tree height:

$A = D2 \times (\tan(a))$ ..... (3.1)

Total tree height (H) = A+B..... (3.2)

Where; D2 = Horizontal distance from the instrument to the foot of the tree, B= Height of the prism rod (target), A = Height of the tree from top of the prism rod, a = Angle of inclination

Figure 3.4: Measurement of sample plot position and tree parameters

Tree Diameter at Breast Height (DBH) was measured for all trees in each sample plot using a measuring tape at the height of 1.3m from the foot of each tree (figure 3.6), tree with DBH less than 5cm were excluded in the study, as stipulated in a study conducted by Kachamba, Ørka, Gobakken, Eid, and Mwase (2016). A total of 63 tree were measured in sample plot1, 24 in sample plot2 and 63 in sample plot3 (figure 3.5). All the measurements were entered in the prepared data sheet for further processing.

(a) (b)

Figure 3.5: Tree composition in (a)Sample plot1 (b) Sample plot3

The measured perimeters were later converted to DBH using equation 3.3 (Blozan, 2006)

$$\frac{P}{\pi} = D \quad \text{..... (3.3)}$$

Assuming that tree stems are circular, where; P = Perimeter, Π =Pi, D= Stem diameter = DBH


Figure 3.6: Measurement of tree stem perimeter

3.4 Data Processing

This section describes the processing of the data with the aim of deriving the input parameters for forest AGB estimation basing on both field inventory and UAV images

3.4.1 Field based data

Field data collected from three sample plots chosen as the representative of the study area entailed tree stem diameters measured at breast height, sample tree heights, and positions of the sample plots. The ranges of measured DBH and selected sample tree heights per sample plot are presented in figure 4.1(a and b respectively).

3.4.2 UAV Images Processing

The raw UAV images are associated with a pose file information that gives the details of camera position information and orientation parameters. The images were processed using Agisoft Metashape Professional software. The software was chosen due to its capability to process UAV

images and produce reliable results through Structure from Motion and image matching algorithms imbedded into the software (Ota et al., 2015)

This study used 66 overlapping images which were loaded into the software together with the pose file where each image was tagged with its corresponding camera position and orientation parameters (Table 3.2). The photographs were assessed for their quality with a threshold of 0.5 units calculated from highly focused part of the image, this is because poorly focused and blurred images influences alignment of the photos and need to be eliminated before processing of the photos (Agisoft, 2019). The assessment showed the quality of all photos loaded was well above the recommended threshold of 0.5 units (Table 3.3). Camera position coordinate system was transformed from world geographic coordinate to projected WGS 84 coordinate system to match with the GCPs coordinate system. Image matching was then executed which resulted into alignment of all the photographs and sparse point cloud. The accuracy for photo alignment was set to high to enhance accuracy in camera positions.

Table 3.2: Part of Camera position and orientation Parameters

Photograph ID	Latitude	Longitude	Altitude(m)	Yaw (◦)	Pitch (◦)	Roll (◦)
DSC00506.jpg	-6.764001	39.214199	403.7	0.2	-1.7	194.2
DSC00507.jpg	-6.764398	39.2141	403.5	1.4	-1.4	194.2
DSC00508.jpg	-6.764831	39.213989	403.4	1.4	-2	193.7
DSC00509.jpg	-6.765261	39.21389	403.4	-0.1	-2.3	192.9
DSC00510.jpg	-6.765692	39.213791	403.4	-0.9	-2	193.6
DSC00511.jpg	-6.766144	39.213673	403.4	1.3	-1.7	194.2
DSC00512.jpg	-6.766576	39.213573	402.8	-0.9	-0.5	192.7
DSC00513.jpg	-6.767007	39.213478	402.4	-1.1	-0.3	193.9
DSC00514.jpg	-6.767432	39.213367	403.2	0.7	-0.9	194.1
DSC00598.jpg	-6.767724	39.214443	404.5	-0.2	-3.7	13.2
DSC00599.jpg	-6.76729	39.21455	405.5	0.8	-6.4	14.5
DSC00600.jpg	-6.766848	39.214664	405.1	1	-7.1	13.8
DSC00601.jpg	-6.766439	39.21476	404.1	0.4	-5.7	13.1
DSC00602.jpg	-6.765973	39.214867	403	-0.5	-3.8	13.4
DSC00603.jpg	-6.765566	39.214962	402	0.3	-2.6	13.6
DSC00604.jpg	-6.765117	39.215073	402.1	1.2	-2.1	14.6
DSC00605.jpg	-6.764723	39.215172	402.5	0	-2.4	14
DSC00606.jpg	-6.76429	39.215275	402.7	-1.5	-3.1	13.4
DSC00607.jpg	-6.763826	39.215385	403.1	0.1	-2.8	13.4
DSC00608.jpg	-6.763413	39.215488	404	-2.1	-5.1	13.2

Table 3.3: Part of image quality assessment report

Photo Label	Size	Aligned	Quality(m)	Camera Make	Focal length
DC00378	7360×4912	Yes	0.878454	SONY	35mm
DC00379	7360×4912	Yes	0.894912	SONY	35mm
DC00380	7360×4912	Yes	0.886013	SONY	35mm
DC00381	7360×4912	Yes	0.864282	SONY	35mm
DC00382	7360×4912	Yes	0.844559	SONY	35mm
DC00383	7360×4912	Yes	0.826887	SONY	35mm
DC00384	7360×4912	Yes	0.829252	SONY	35mm
DC00385	7360×4912	Yes	0.836158	SONY	35mm
DC00386	7360×4912	Yes	0.833639	SONY	35mm
DC00387	7360×4912	Yes	0.847713	SONY	35mm
DC00388	7360×4912	Yes	0.857505	SONY	35mm
DC00389	7360×4912	Yes	0.800688	SONY	35mm
DC00391	7360×4912	Yes	0.848674	SONY	35mm
DC00392	7360×4912	Yes	0.879462	SONY	35mm

To enhance the generated model accuracy, GCPs were imported for georeferencing. The software uses markers to optimize photo alignment and therefore each GCP marker was manually dragged and placed on the appropriate position on the overlapping photos. This georeferencing process removes linear errors that occurred during photo alignment, the non-linear component of the errors is removed by Camera optimization process (Agisoft, 2019). Optimization parameters namely focal lens of the camera, principal point coordinates, skew transformation, radial distortion and tangential distortions were all checked and finally the model was updated.

3.4.3 Dense point Cloud

A total of 66 images taken at a flying altitude of 409m with ground resolution of 5.4cm/pix and covering area of 0.743km² were processed resulting into a dense point cloud of 117,988,013 points. The Root Mean Square Error (RMSE) of the tie points averaged over all images used in the study area was 1.24 pix (Table 3.4). The RMS reprojection error was 0.186236 (1.24246 pix) with the maximum projection error of 1.02897 (26.7898 pix).

The calibration coefficients and correlation matrix for the parameters f, cx, cy, b1, b2, k1, k2, k3, k4, p1, p2, p3, and p4 (Agisoft, 2019) are shown in table 4.2 where f= focal length of the camera, cx, cy = Principal Coordinates, b1, b2 = non-orthogonal transformation coefficients, k1, k2, k3, k4 = radial distortion coefficients, p1, p2, p3, p4 = tangential distortion coefficients.

Appendix 1.4 presents deviation and correlation values of the parameters used in the bundle adjustment and dense image matching. No external parameters were imported and therefore the correlation values are from the internal camera orientation parameters that portray the degree of correlation of the respective parameters. The standard deviation for the camera position and rotation angles are shown by the positive diagonal elements of the covariance matrix and the average camera location error is shown in Table 3.5 and the camera locations as presented in Figure 3.7 as well.

Table 3.4: Camera and image details

Camera Model	Resolution		Focal Length	Pixel Size	Pre-calibrated
ILCE-7R (35mm)	7360 x 4912		35 mm	4.89 x 4.89 μm	No
Number of images: 66 Flying altitude: 409 m Ground resolution: 5.4 cm/pix Coverage area: 0.743 km²			Camera stations: 66 Tie points: 66,844 Projections: 252,955 Reprojection error: 1.24 pix		

Table 3.5: Average camera location error

X error (m)	Y error (m)	Z error (m)	XY error (m)	Total error (m)
1.80339	7.77842	46.4167	7.98474	47.0985

Figure 3.7: Camera locations

The estimation of internal and external camera orientation parameters during photo alignment comes with errors in the estimates. The alignment process is influenced by overlap of the adjacent images and the shape of the features surface resulting into non-linear deformation of the generated model to some extent. Linear transformation of the model with the 7 transformation parameters used for translation, similarity, rotation and scaling, during model georeferencing cannot resolve the nonlinear deformations, rather errors due to linear misalignment. The non-linear deformation is dealt with by camera optimization process that refers on the GCPs to adjust the point cloud.

The algorithm that implements optimization in Metashape adjusts the estimated point coordinates and camera parameters thereby minimizing the projection errors (Agisoft, 2019).

The individual GCPs and check points projection error estimates is presented in Table 3.6 and 3.9 while the overall GCPs and check points projection root mean square error is presented in Table 3.7 - 3.8

Table 3.6: Individual Ground Control Points projection error

GCP id	X error (cm)	Y error (cm)	Z error (cm)	XY error (cm)	Total (cm)
CA09	-2.30932	2.5952	-2.61526	4.34829	0.456 (10)
CP3	0.185934	3.35203	0.621135	3.41415	0.345 (15)
GCP32	1.8263	2.22954	-2.09997	3.56596	0.216 (7)
PT01	-0.55312	-0.596579	-2.33715	2.47469	0.497 (8)
PT02	-0.537146	-1.51647	3.83567	4.1594	0.470 (8)
PT04	-2.044	1.0113	4.28248	4.85183	0.330 (8)
PT11	1.43105	-6.89481	-2.44427	7.45391	0.629 (18)
PT13	3.08309	2.33369	1.66359	4.20941	0.863 (17)
T1	-1.49525	-1.70018	-0.756278	2.38712	0.282 (8)
BB2	2.67047	4.03173	1.17466	4.97655	0.440 (13)
BB3	3.79043	-4.39376	-3.28248	6.66687	0.552 (9)
BB4	-7.68743	-0.0670433	4.56362	8.94023	0.480 (10)
Total	2.99805	3.13661	2.77556	4.33897	5.15076

Table 3.7: Overall Ground Control Points projection RMSE

Count	X error (cm)	Y error (cm)	Z error (cm)	XY error (cm)	Total (cm)
12	2.99805	3.13661	2.77556	4.33897	5.15076

Table 3.8: Overall Check Points projection error RMSE

Count	X error (cm)	Y error (cm)	Z error (cm)	XY error (cm)	Total (cm)
3	6.62782	5.87733	12.2365	8.85838	15.1063

Table 3.9: Individual Check Points projection error

CP id	X error (cm)	Y error (cm)	Z error (cm)	XY error (cm)	Total (cm)
GCP30	9.02448	3.63616	-13.848	16.9243	0.356 (17)
T2	-4.02101	1.44516	16.0444	16.6037	0.372 (2)
BB1	-5.84585	9.39782	0.013915	11.0677	0.306 (11)

Total	6.62782	5.87733	12.2365	8.85838	15.1063

3.4.3 Point cloud classification

Recent development in automated ground filtering algorithms based on machine learning and implemented in various software has enabled automated classification of point cloud data into multiple classes for considerable short time and to a reasonably good accuracy, therefore generation of reliable DSM and DEM (Chen et al., 2016). In this study, the parameter settings for quality were set to high to get accurate results, and the filtering mode set to moderate taking in consideration the processing time. The generated point cloud was classified into six classes namely bare ground, roads, vegetation, building, man-made objects and cars based on geometric and colour information (Agisoft, 2019). The classification was performed with the main target being to discriminate trees and the bare ground from the rest of the objects and form their independent classes (figure 3.8). Pesso, Amorim, and Galo (2018), Özdemir and Remondino (2019) however, admits the complexity in the discrimination of urban scene point cloud data that multiple objects comprised of natural and man-made are represented by the data using automatic approaches, to this end robust algorithms are needed to minimize the classification errors. Visual inspection of the classification results as it appears in figure 4.4 was convincing to have successfully discriminated the forest and the bare ground from other objects.

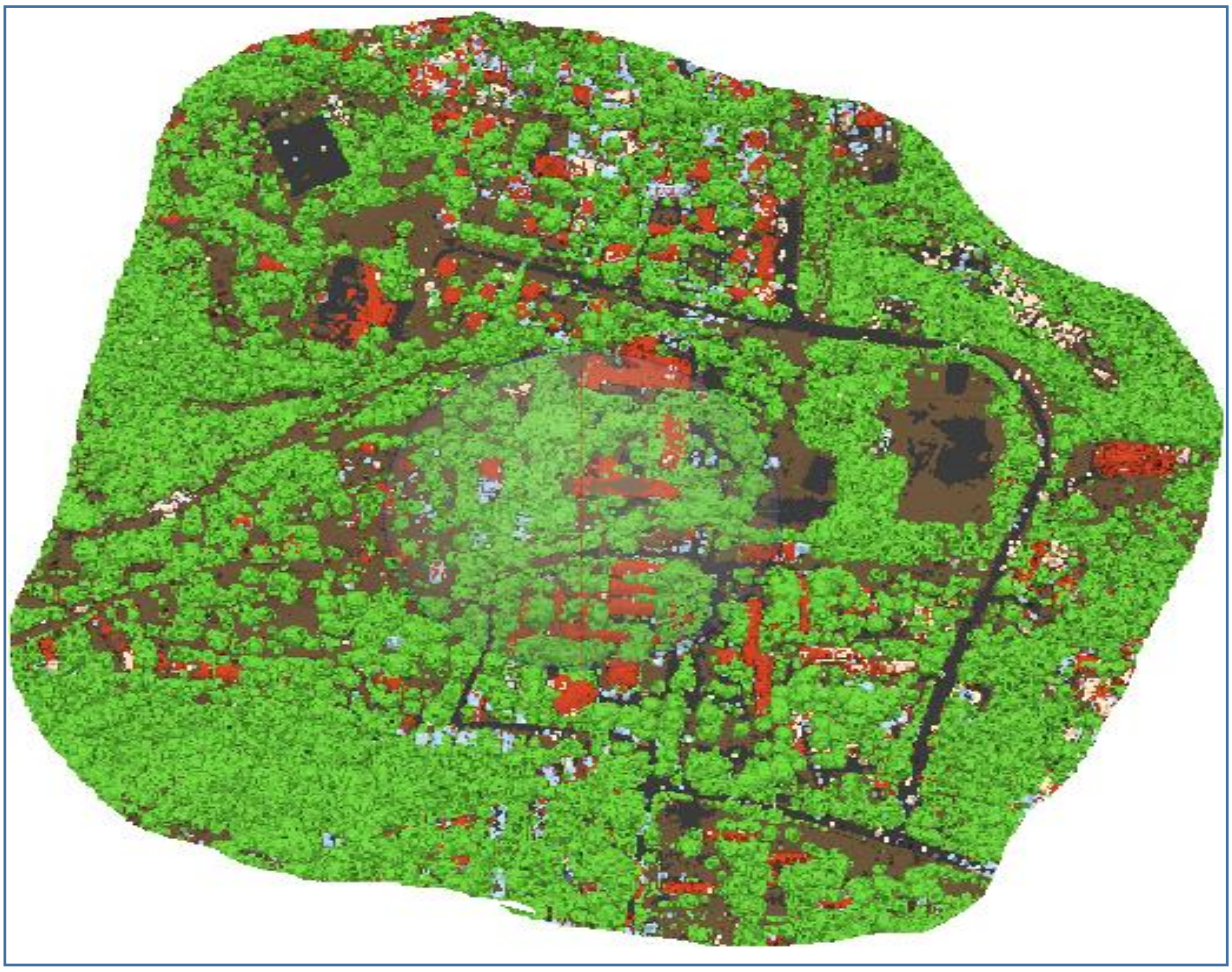

Figure 3.8: Dense point cloud classification

3.4.4 DSM, DEM and Mosaic generation

DSM was generated using the vegetation class whose data represented the top of the forest canopy (figure 4.3a). DEM was generated using the bare ground class with the interpolation mode enabled to interpolate the ground points at locations where point density was sparse due to tree canopies (Figure 4.3b). This approach was also used in a study conducted by Kachamba et al. (2016).

Two other important facts were taken into consideration regarding the capability of UAV images to capture much information of the ground under forest canopies (i) the study area is not covered by dense tree canopies (ii) the images were taken on an off-leaf season in September.

The ortho-mosaic of the study area with pixel size of 5cm was then generated using 66 images that covered the study area (Figure 4.2) and was used to delineate individual tree crowns

3.4.5 Canopy height models

To extract tree heights, canopy height models were generated as the difference between DSM and DEM using equation 3.4 (NOAA, 2012; Ota et al., 2015).

CHM = DSM – DEM …… (3.4)

Where: CHM = Canopy Height Model, DSM = Digital Surface Model, DEM = Digital Elevation Model. The DSM represents the top of tree canopy and DEM represents the foot of trees. Four CHMs were generated using QGIS packages version 3.8, where the three CHMs represents for the sample plots as shown on Figure 4.4(a, b, c) and one CHM covering the overall study area (Figure 4.4d). The CHMs were clipped to individual sample plot raster for further analysis

3.4.6 Sample plot tree crown delineation

Tree crowns delineation for the sample plots was done from respective image mosaics aiming at creating individual tree crown polygons. Image mosaics were chosen for crown delineation because manual delineation is even simple as objects appear clearer as compared to canopy height model raster (Figure 3.9a). Sample plots CHM raster were then overlaid with their respective tree crown polygon shapefiles to extract tree heights (Figure 3.9b). The maximum value of each tree crown was generated and the data were merged with their corresponding crown areas. The attribute information was used further analysis.

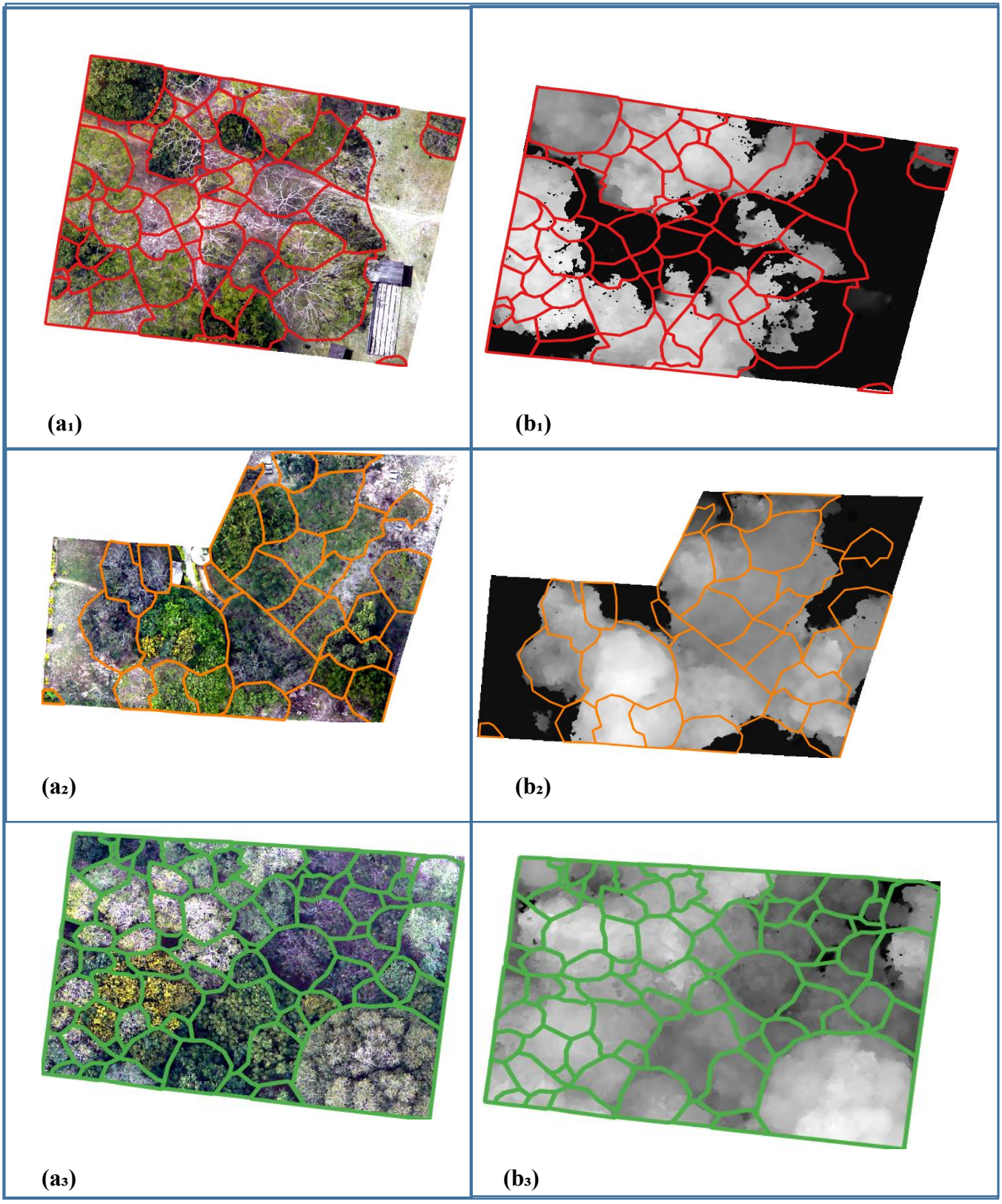

Figure 3.9: (a) delineated sample plot mosaic (b) Sample plot CHMs overlaid with tree crown polygons

3.4.7 Image Segmentation

Image segmentation was implemented to delineate individual tree crowns for the overall study area. The technique was implemented using multi-resolution algorithm which uses the bottom up regional merging technique where image pixels are merged basing on the principle of minimizing heterogeneity meanwhile maximizing similarity (Baatz & Schäpe, 2000). The derived tree crowns were used to extract tree heights and predict DBH as important parameters for forest above ground biomass estimation. Similar approaches were also employed by Ibrahim and Osman (2014) for extracting tree parameters, to this end, the mosaic covering the study area was segmented and the results were visually assessed on the mosaic (Figure 4.2). Then Excess Green Index (ExGI), as shown on figure 4.6, was computed and used to discriminate vegetation from other objects. ExGI is among the best contrast based vegetation discrimination index and its performance is parallel to NDVI (Asier & Lluis, 2019). The segmented image mosaic was classified into three classes basing on ExGI values to discriminate tree crowns from other objects like bare land, roads and buildings. Equation 3.5 was used to compute ExGI (Avola et al., 2019).

$$ExGI = 2*G - (R+B) \quad \ldots\ldots (3.5)$$

Where ExGI = Excess Green Index, G = Green band, R= Red band, B= Blue Band. The tree crown polygons covering the study area were then overlaid on the corresponding CHM (Figure 3.9) to extract tree heights.

3.4.8 Tree Variables extraction

Tree heights, crown area and crown diameter were the only variables extracted from the segmented canopy height models. Tree heights were extracted by taking the maximum pixel value of each tree crown in the segmented canopy height models. The segmentation results were used for further analysis. Diameter at breast height is the parameter not easily extracted from UAV images and this is because of the inability of UAV photographs to capture much details below the canopies as lower parts are obscured by the crowns (Guerra-Hernández et al., 2017). Different models has been developed to predict diameter at breast height from UAV images (Ibrahim & Osman, 2014). The study utilizes the models developed by Mahmut (2004), Lawrence (1995) and Batbaatar et al. (2019) to extract DBH, equation 3.6 and 3.7.

$$DBH = a_o + a_1(CD) \quad \text{(3.6)}$$

$$DBH = a_o CD^{a_1} \quad \text{(3.7)}$$

Where DBH = Diameter at breast height, CD = Crown diameter, a_o and a_1 are regression coefficients. A research conducted by Penggang, Kai, Chen, Hailin, and Yinhui (2019) highlights that tree crown is the essential parameter that can be used to derive models for DBH prediction. In this study tree crown polygon areas were computed using QGIS 3.8 package and tree crown diameters, were computed from crown areas using equation 3.7 (Lim et al., 2015).

$$D = \sqrt{\left(\frac{4A}{\pi}\right)} \quad \text{(3.8)}$$

Where D = Crown diameter, A = Crown area

3.5 AGB estimation

AGB estimation was done at tree level from the two datasets acquired from field inventory and those extracted from UAV images. As for field inventory data, DBH and mean tree height for each sample plot was used to estimate individual tree biomass and plot level biomass was obtained as the summation of individual tree biomass. The same approach was applied for data extracted from UAV images but in this case each polygon had its respective maximum pixel value representing tree heights. The allometric models (equation 3.9 and3.10) as compiled by Malimbwi et al. (2016) and Munishi et al. (2008) were used for AGB estimation of the study area for all datasets.

$$AGB = 0.1711 \times (DBH)^{2.0047} \times ht^{0.3767} \quad \text{(3.9)}$$

$$AGB = 0.5927 \times DBH^{1.8316} \quad \text{(3.10)}$$

Where AGB = Above ground biomass, DBH = Diameter at breast height, ht = Tree height. Equation 3.10 is opted when DBH is used as the only input into the model.

3.6 Validation of the results

AGB estimated basing on the field inventory data was regarded as the most accurate (Temesgen et al., 2015) and therefore was used as a comparison to AGB estimated from UAV images.

Statistical tests were employed to compare the variables extracted from UAV images and the field inventory data. Furthermore, equations 3.11(Jucker et al., 2017) and 3.12 (W.A Mugasha et al., 2015) were used to evaluate the accuracy of the employed AGB estimation method.

$$RMSE = \sqrt{\frac{1}{N}\sum_{i=1}^{N}(AGB_{o} - AGB_{p})^{2}} \quad \text{..... (3.11)}$$

$$\text{MPE} = \frac{100}{n} \times \Sigma \left(\frac{Y - Yi}{Yi}\right) \times 100 \quad \text{..... (3.12)}$$

Where RMSE = Root mean square error, N = Sample size, AGB_{o} = Observed AGB, AGB_{p} = Predicted AGB, MPE = Mean Prediction Error, Y= Predicted AGB, Yi = Measured AGB

CHAPTER FOUR

RESULTS AND DISCUSSION

4.1 Overview

The chapter presents the results and discussion of the research activities with regard to the specific objectives. Statistical approached was used to analyze the results and finally validation was done by comparing AGB estimated using UAV images with that estimated using field collected data.

4.2 Field based DBH and tree height

The ranges of measured DBH and selected sample tree heights per sample plot are presented in figure 4.1a-b, where the minimum and maximum DBH were 11.46cm and 111.41cm for plot1, 5.09cm, 89.46cm for plot2, 5.09cm and 101.85cm for plot3 with mean DBH of 36cm, 41.35cm and 26.32cm respectively (Figure 4.1a).

At least ten trees were randomly selected for height measurement in each sample plot. The mean tree height measured in sample plot1 was 14.61m, 10.27m in sample plot2 and 11.67m in sample plot3 as presented in Figure 4.1b

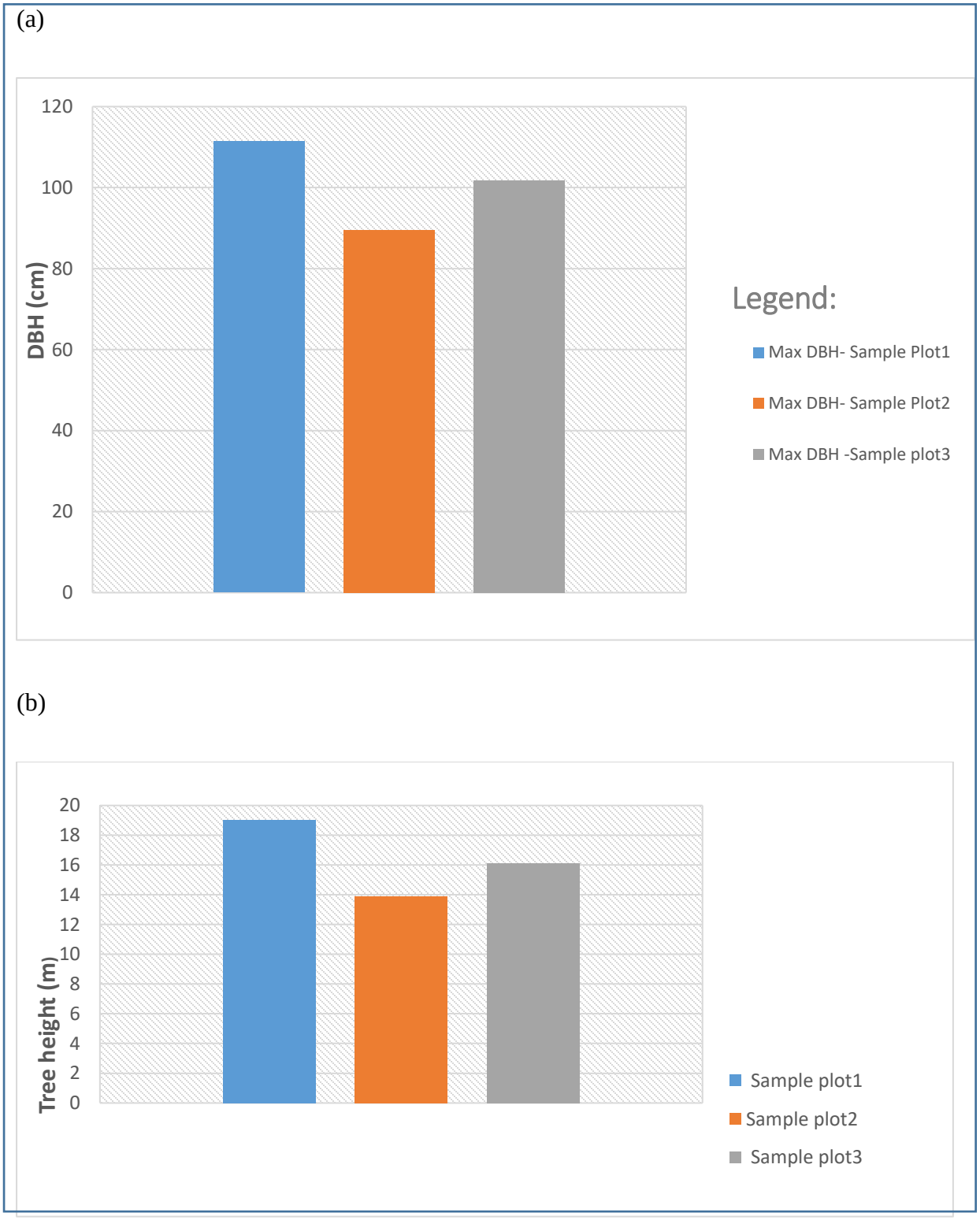

Figure 4.1: Distribution of measured (a) DBH (b) tree height

4.3 UAV based extracted information

Various information was extracted from UAV images at different processing stages. DSM, DEM, CHM and ortho mosaic were generated for use in subsequent sequence of processes that led to estimation of AGB.

4.3.1 Ortho mosaic

A two-dimension full resolution ortho mosaic in original RGB color bands was generated to display the continuous surface onto which results of the processing stages are based (Figure 4.2). It was generated based on the DSM with mosaic Blending mode. The ortho mosaic was segmented and classified into 3 classes (Figure 4.5) to filter out buildings and other man-made features. Further analysis was carried out by computing Excess Green Index on the vegetation class where small trees were filtered out basing on attained values (Figure 4.6). The tree crowns generated by polygons using the filtered vegetation class was finally overlaid on the CHM to extract tree heights (Figure 4.7)

4.3.2 DSM, DEM and CHM

The elevation ranges for the DSM is between 32.59m and 103.36m and for the DEM elevation range is between 32.11m and 93.90m above mean sea level. Subtraction of the DEM from DSM resulted in CHMs with height ranging between 0m-30m for the overall study area (Figure 4.4d). The tree height range for sample plot1 is between 0m and 18.47m (Figure 4.4a) while in sample plot2, tree height ranges between 0m-14.63m and between 0m-18.63m (Figure4.4b), for sample plot3 (Figure 4.4c).

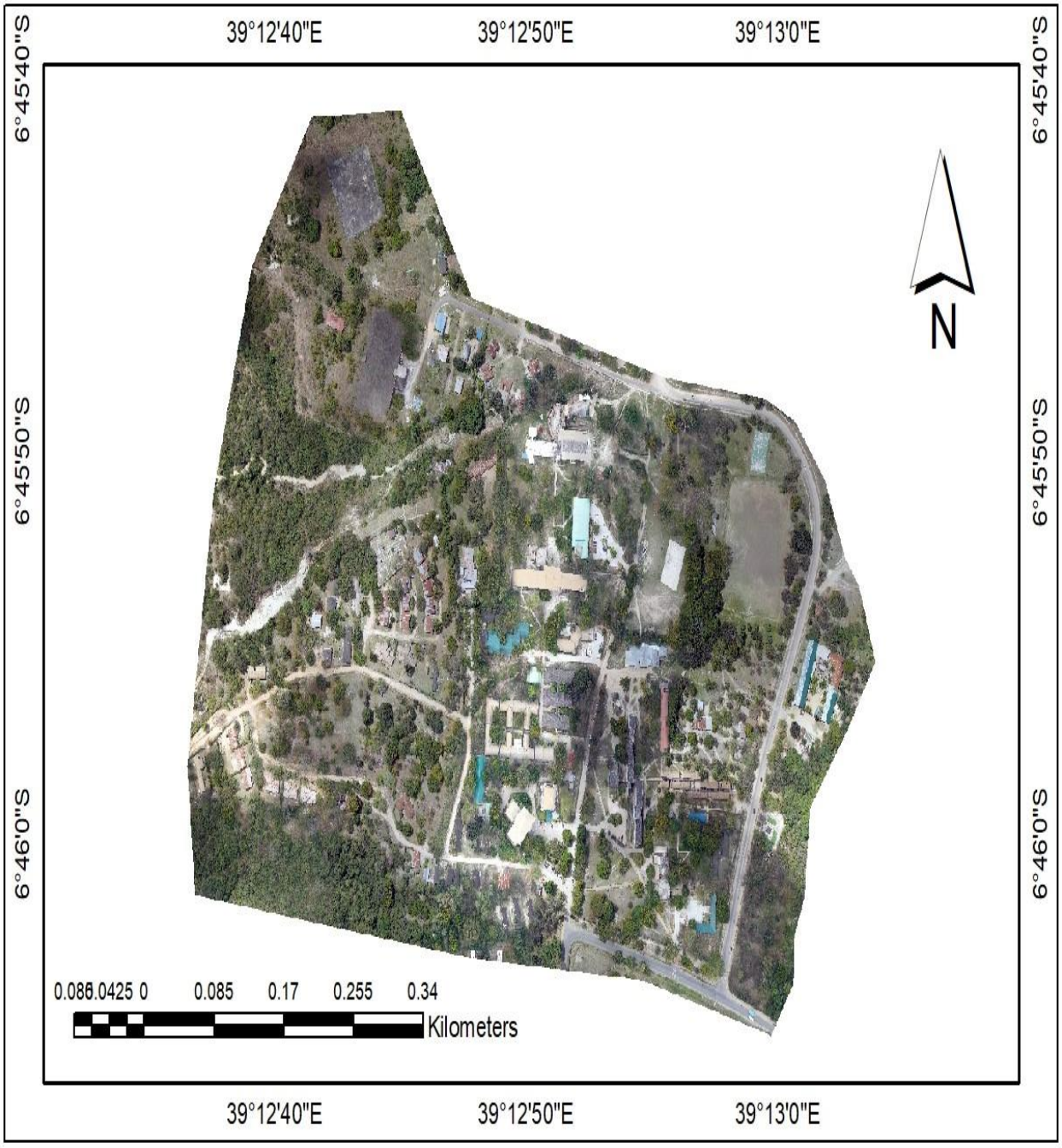

Figure 4.2: Ortho mosaic view

(a)

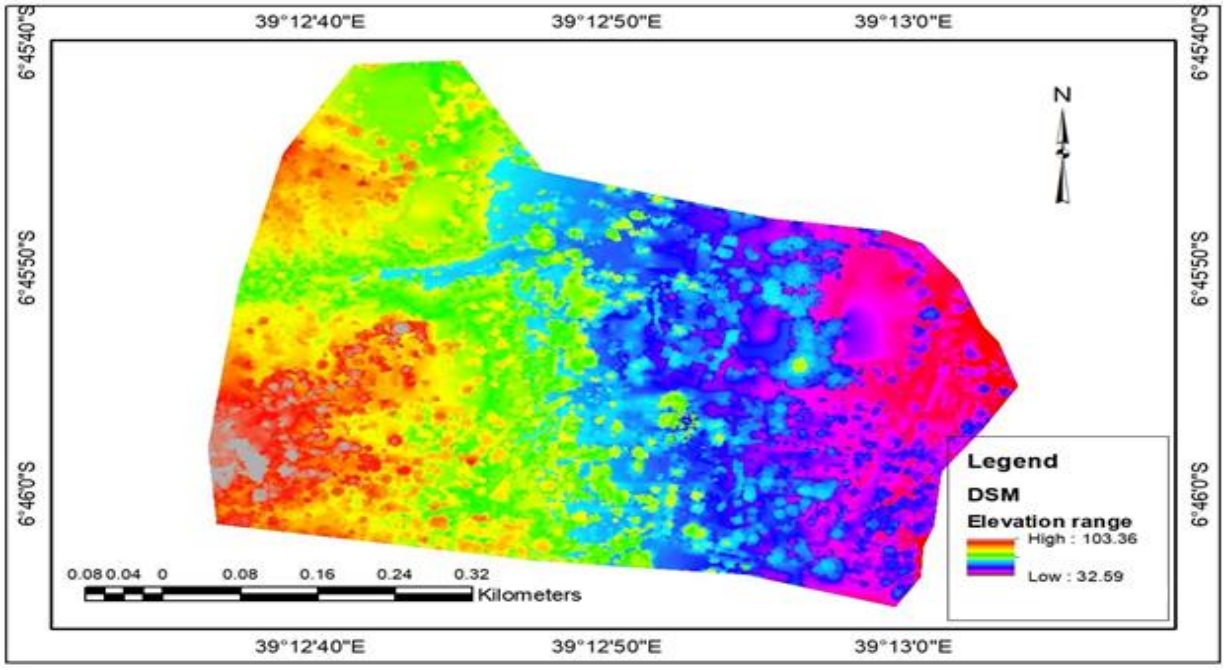

(b)

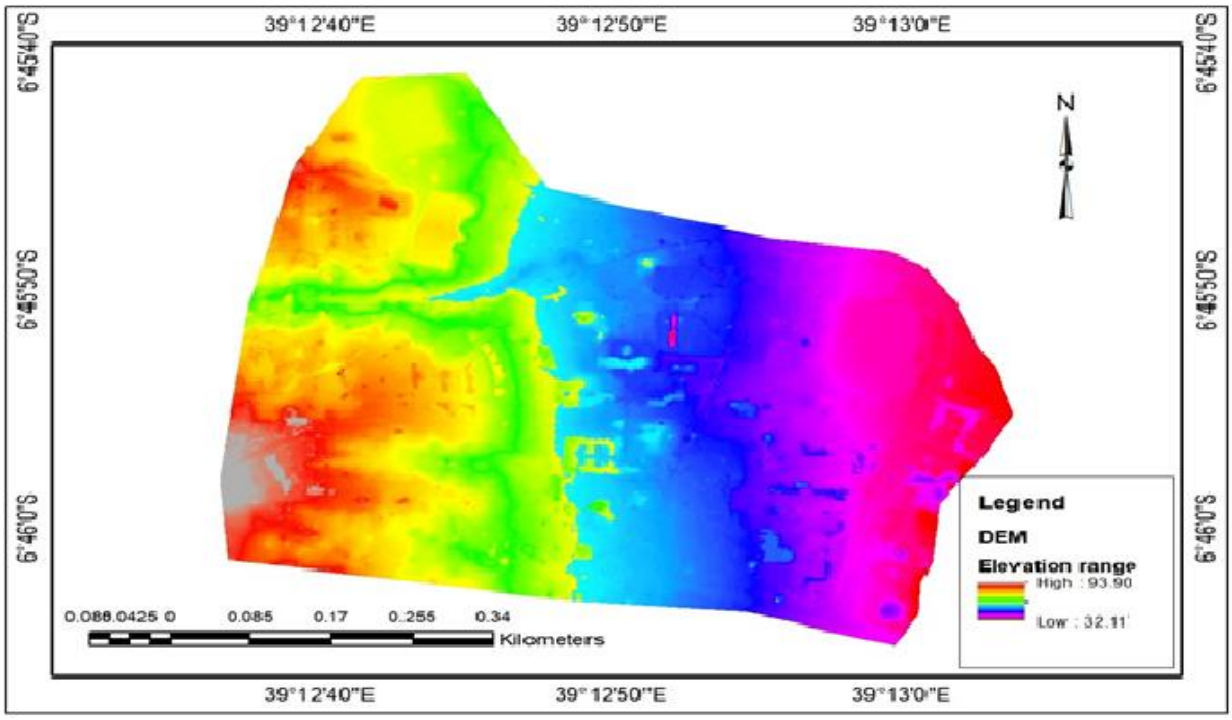

Figure 4. 3:(a) DSM (b) DEM

(a)

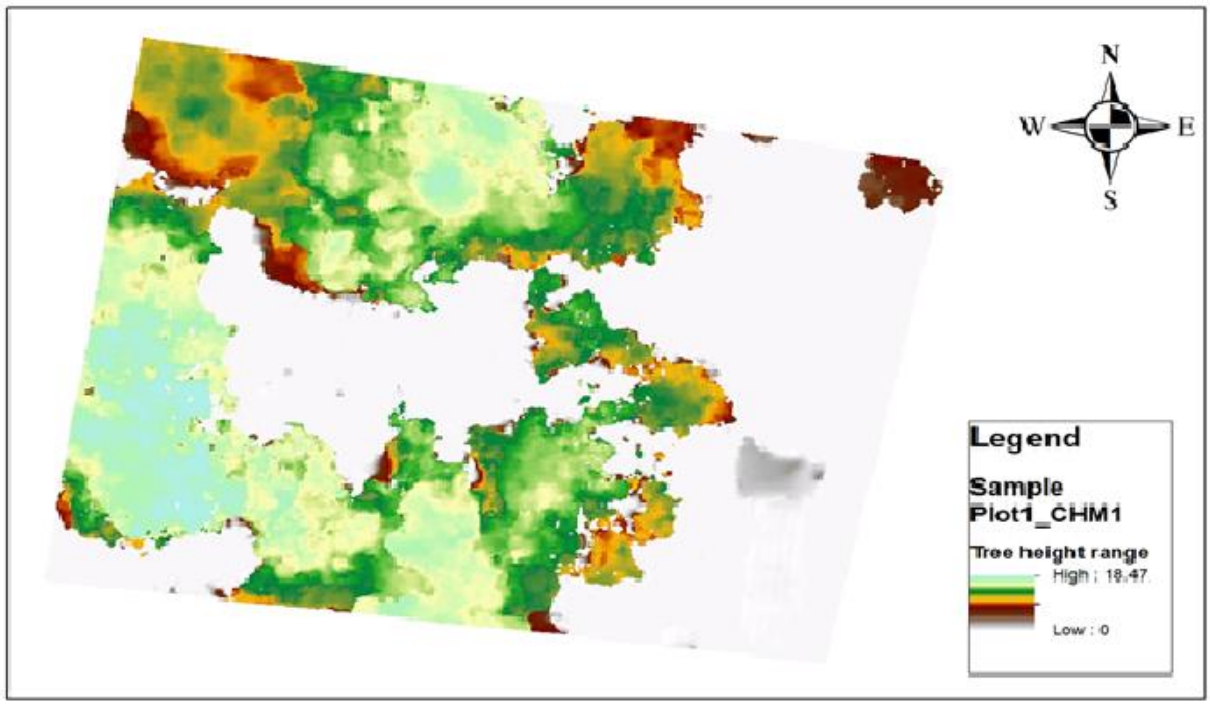
N
W
E
S
Legend
Sample
Plot1_CHM1
Tree height range
High : 18.47
Low : 0

(b)

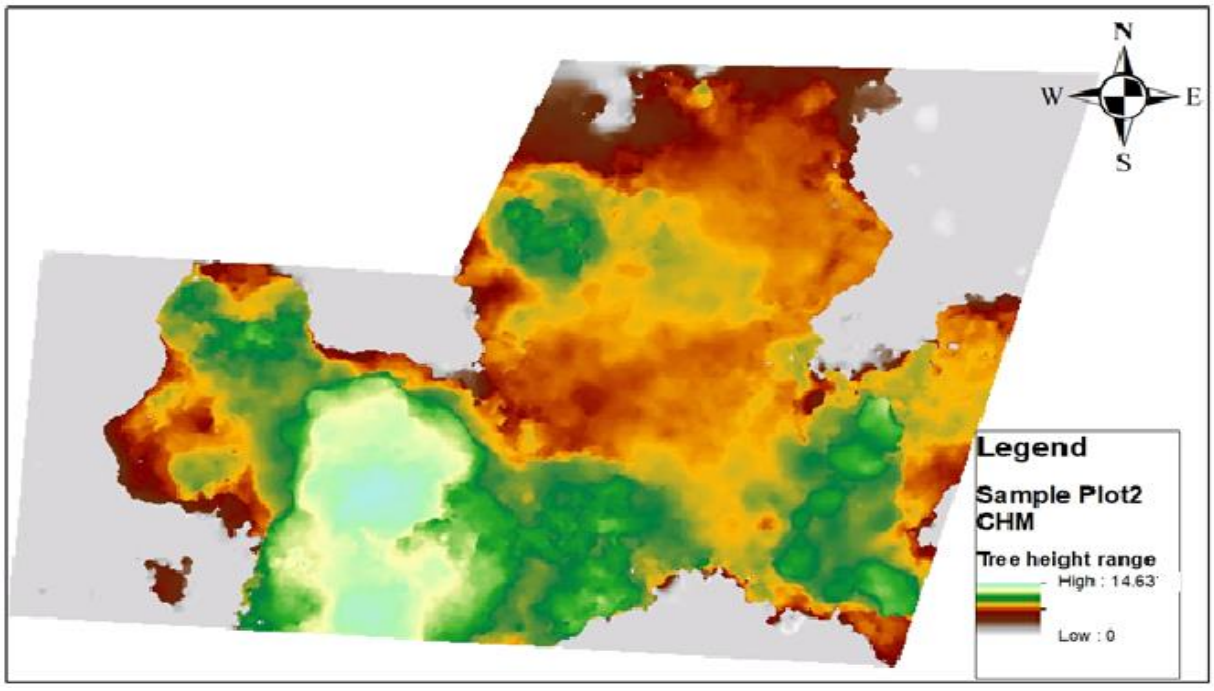
N
W
E
S
Legend
Sample Plot2
CHM
Tree height range
High : 14.63
Low : 0

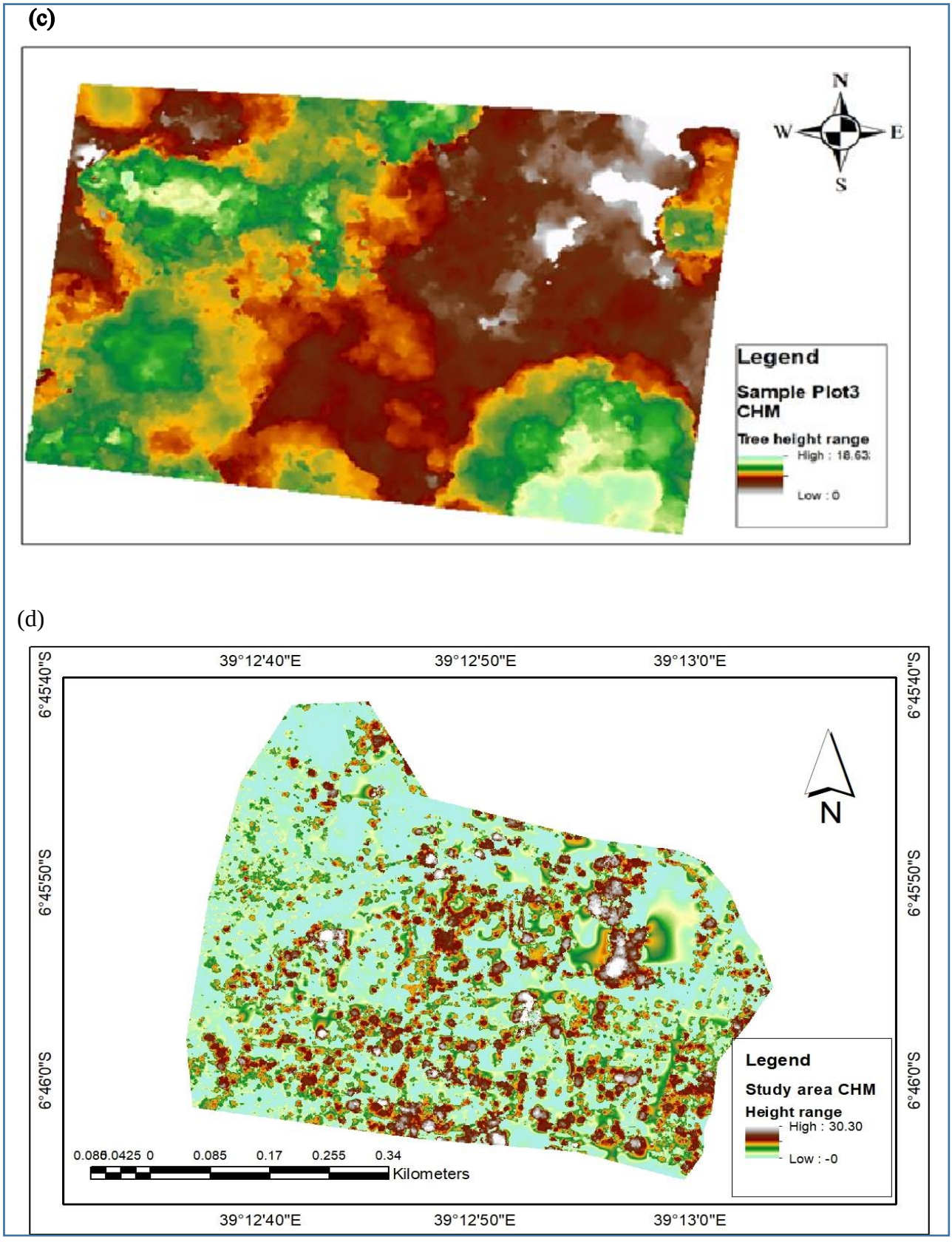

Figure 4.4: CHMs for (a) Sample plot1 (b) Sample plot2 (c) Sample plot3 (d)Overall study area

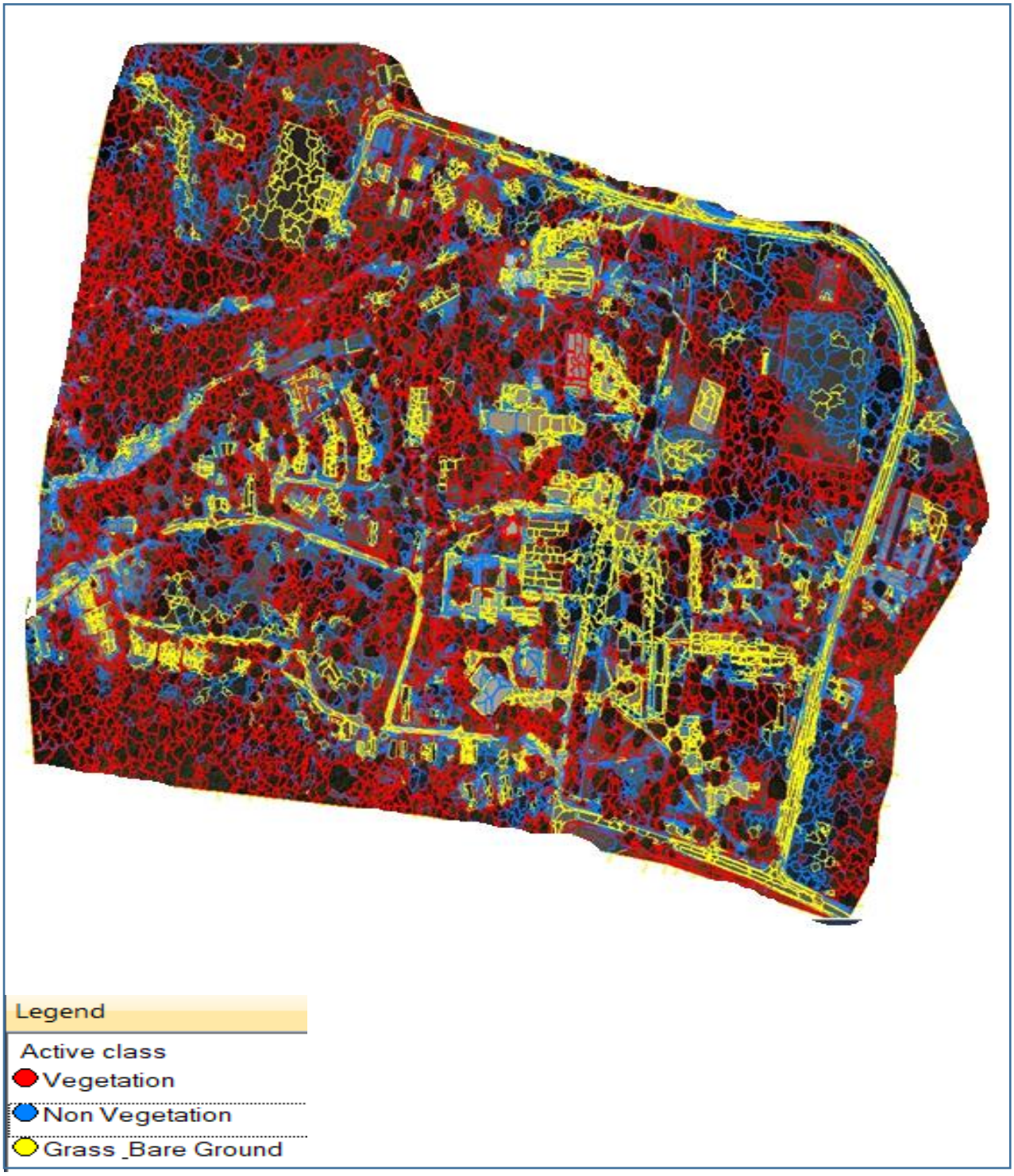

Figure 4.5: Classification of the segmented mosaic

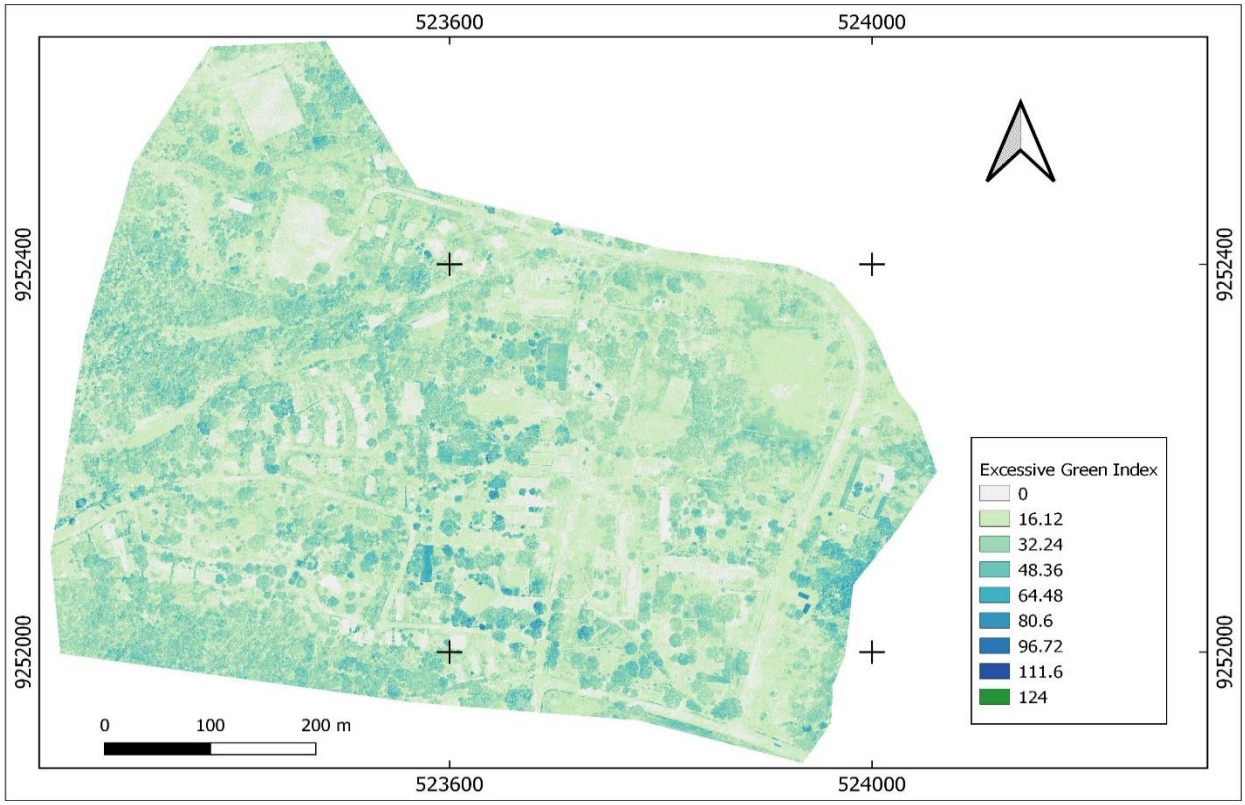

Figure 4.6: Excess Green Index

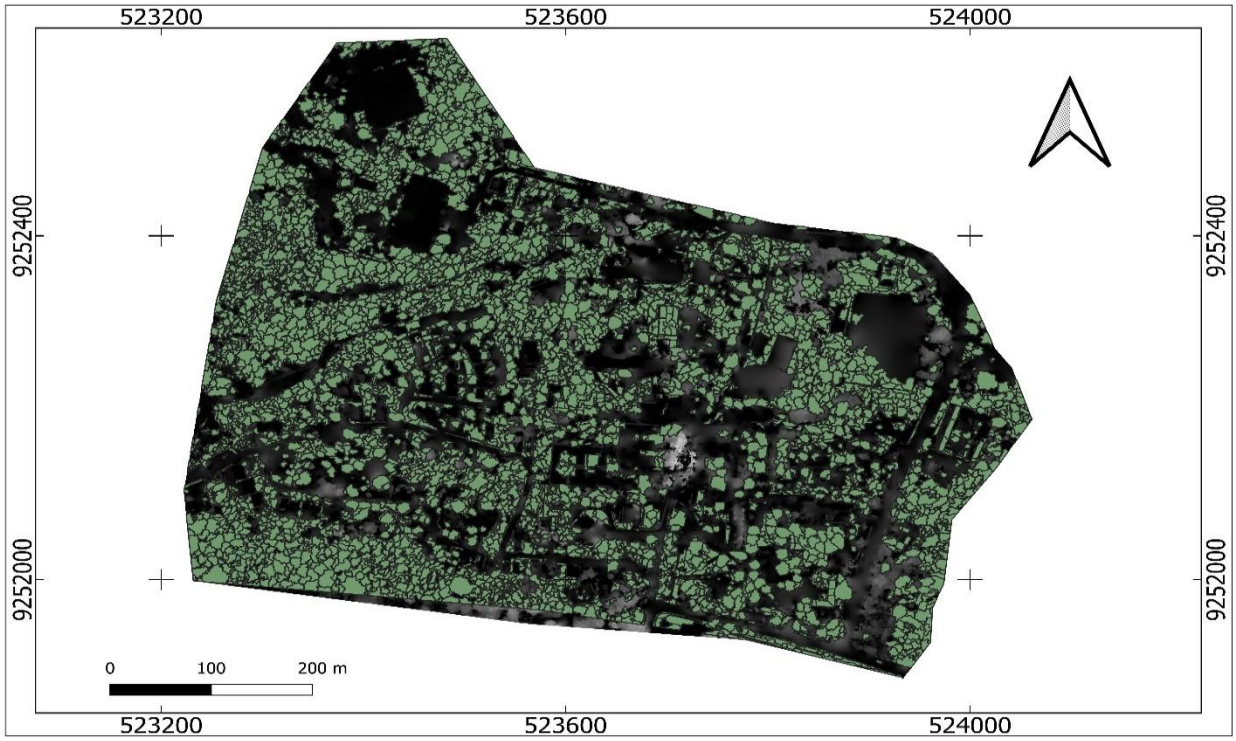

Figure 4.7: Tree crown polygons overlaid on the CHM

4.3 Statistical analysis

Statistical analysis was performed as a standard procedure to compare the results of the analyzed variables. In this study, one of the objectives was to compare the AGB estimated using field data and the corresponding AGB estimated based on UAV images.

4.3.1 Descriptive statistics for sample plots inventory data

The descriptive statistics for measured DBH and tree heights for all sample plots as explained in section 3.4.3 are presented in Table 4.8 and able 4.9 respectively.

Table 4.1: Descriptive statistics for the measured tree DBH

	Sample plot1(cm)	Sample Plot2(cm)	Sample Plot3(cm)
Mean	36.844	41.353	26.327
Standard Error	3.079	3.953	2.090
Standard Deviation	24.241	18.958	16.723
Sample Variance	587.602	359.405	279.669
Minimum	11.459	5.093	5.093
Maximum	111.408	89.464	101.859
Observation	63	24	64
Confidence Level (95.0%)	6.156	8.198	4.177

Table 4.2: Descriptive statistics of the measured tree height samples

	Sample Plot1(m)	Sample Plot2(m)	Sample Plot3(m)
Mean	14.605	10.271	11.665
Standard Deviation	3.957	2.560	3.422
Sample Variance	15.662	6.553	11.711
Minimum	6.572	7.029	5.823
Maximum	19.044	13.888	16.120
Sample Size	11	10	9
Confidence Level (95.0%)	2.831	1.968	2.861

4.3.2 Descriptive Statistics for the UAV derived data

The tree heights and diameter at breast heights derived from the processed UAV images were also statistically analyzed for each sample plot and the overall study area as presented in table 4.10, table 4.11 and table 4.12.

The minimum and maximum predicted DBH for sample plot1 having 63 samples was 38.26cm and 48.5cm respectively with the mean predicted DBH value of 44.13cm and standard deviation 2.28cm while sample plot2 with 24 tree crown samples, the minimum and maximum DBH were 32.43cm and 48.20cm respectively, mean value of 41.37cm and standard deviation of 3.93cm. For Sample plot3 with 65 trees, the minimum and maximum predicted DBH were 10.12cm and 46.60cm respectively, the corresponding mean and standard deviation were 24.57cm and 7.27cm respectively (table 4.10)

Table 4.3: Descriptive Statistics of the predicted tree DBH

	Sample Plot1(cm)	Sample Plot2(cm)	Sample Plot3(cm)
Mean	44.128	41.372	24.566
Standard Error	0.290	0.820	0.908
Standard Deviation	2.280	3.930	7.267
Sample Variance	5.197	15.447	52.807
Minimum	38.257	32.428	10.120
Maximum	48.501	48.195	46.595
Sample Size	63	24	65
Confidence Level (95.0%)	0.579	1.700	1.815

Table 4.4 gives a summary of sample plots derived tree height statistics where in sample plot1, the minimum and maximum tree heights were 6.0m and 18.48m respectively. The mean tree height was 13.57m and standard deviation 2.66m while for sample plot2 the minimum and maximum heights were 7.73m and 14.61m respectively. The corresponding mean was 10.70 and standard deviation was 2.08m. Minimum and maximum heights derived for sample plot3 were 6.47m and 17.80m respectively where the mean height was 13.36m and standard deviation being 2.62m

Table 4.4: Descriptive Statistics of the derived tree height

	Sample plot1(m)	Sample Plot2(m)	Sample Plot3(m)
Mean	13.567	10.704	13.365
Standard Error	0.338	0.442	0.328
Standard Deviation	2.659	2.075	2.623
Sample Variance	7.069	4.304	6.879
Minimum	5.996	7.733	6.474
Maximum	18.478	14.613	17.795
Sample size	62	22	64
Confidence Level (95.0%)	0.675	0.920	0.655

Table 4.5 presents the summary of statistical analysis performed on derived tree heights and predicted DBH for the overall study area with sample size of 2929 trees.

Results shows that the minimum and maximum derived tree heights were 3.20m and 20.87m respectively giving a height range of 17.67m. The derived mean tree height was 9.59m while the standard deviation was found to be 3.63m.

On the other hand, the predicted DBH was between the minimum value of 26.06cm and the maximum value of 67.77cm, giving a DBH range of 41.71cm. The mean DBH was 36.87cm and the standard deviation was 5.31cm.

Table 4.5: Descriptive statistics for tree height and DBH

	Derived Tree height(m)	Predicted DBH (cm)
Mean	10.200	16.340
Standard Error	0.057	0.019
Standard Deviation	3.112	1.034
Sample Variance	9.684	1.069
Sample size	2929	2929
Confidence Level (95.0%)	0.113	0.037

4.4 Comparison between measured and extracted parameters

The DBH and tree heights extracted from UAV images were validated by comparing them to those collected by field methods.

4.4.1 Statistical tests

Paired two sample t-tests were conducted to test if there were any significant differences between the sample plots mean DBH measured on site and that predicted from UAV images.

Results (table 4.8) shows that there is no significant difference between mean DBH from site inventory data and mean DBH predicted from UAV images in sample plot1 as t critical two tail > t stat(P>0.05). For sample plot2, results also shows that there is no significant difference between the mean DBH from site inventory data and mean DBH predicted from UAV images t stat < t critical two tail (P>0.05). Likewise results for sample plot3 shows no significant difference between the mean DBH computed from field inventory data and the mean DBH predicted from UAV images: t stat < t critical two tail (P>0.05) as shown in table 4.13

Table 4.6: Sample plot DBH Paired Two Sample for Means

	Sample plot1 DBH		Sample plot2 DBH		Sample plot3 DBH	
Statistics	Field DBH	UAV DBH	Field DBH	UAV DBH	Field DBH	UAV DBH
t Stat	-2.344		-0.005		0.752	
P(T<=t) one-tail	0.011		0.498		0.228	
t Critical one-tail	1.670		1.717		1.669	
P(T<=t) two-tail	0.022		0.996		0.455	
t Critical two-tail	2.000		2.074		1.998	

Two sample t tests assuming unequal variances were conducted for all sample plots to see if there were any significant differences between the mean tree height for the randomly selected sample trees and the mean tree height extracted from UAV images. Results shows that, in all sample plots,

no significant differences between the mean tree height measured on site and mean tree height derived from UAV images were observed, as s Stat<t critical two tail (P>0.05). Summary of the t test results are presented in Table 4.7

Table 4.7: Two-Sample for mean tree height assuming Unequal Variances

	Sample plot1 tree heights		Sample plot2 tree heights		Sample plot3 tree heights	
	Field	UAV	Field	UAV	Field	UAV
t Stat	0.923		-0.612		-1.130	
P(T<=t) one-tail	0.187		0.275		0.144	
t Critical one-tail	1.782		1.753		1.833	
P(T<=t) two-tail	0.374		0.549		0.288	
t Critical two-tail	2.179		2.131		2.262	

4.5.2 Above Ground Biomass Estimation

The above ground biomass estimated on the overall study area from 2929 trees detected in the UAV images had the mean of 0.099 t/ha and standard deviation of 0.011 t/ha.

Table 4.8: Descriptive Statistics of estimated AGB

	Estimated Biomass(t/ha)
Mean	0.112
Standard Error	0.001
Standard Deviation	0.027
Sample Variance	0.001
Minimum	0.081
Maximum	0.155
Sum	290.446
Count	2929
Confidence Level (95.0%)	0.001

4.7 Validation of the results

Validation of the results was carried out by comparing the AGB estimated from UAV images to AGB estimated using field collected data. The comparison was done for each sample plot using descriptive statistics, and t-tests together with RMSE which was computed to assess the accuracy of the prediction method employed.

4.7.1 Comparison of the estimated AGB on the sample plots

Table 4.9 presents a summary of descriptive statistics of estimated AGB on the sample plots. Comparing the results, the total AGB estimated from field inventory data in sample plot1 was 36.269 t/ha and that estimated from UAV images was 38.604 t/ha. In sample plot2, the total AGB estimated from field inventory data was 14.93 t/ha and the total AGB estimated from UAV images was 13.123 t/ha, while total AGB estimated from field inventory data in sample plot3 was 20.092 t/ha when compared to the total of 15.932 t/ha estimated from UAV images. The mean biomass from field inventory data in sample plot1 was 0.576 t/ha with standard deviation of 0.704 t/ha, while the mean AGB from UAV images was 0.613 t/ha giving a standard deviation of 0.057 t/ha. Likewise, mean AGB from field inventory data in sample plot2 was 0.622 t/ha and the corresponding standard deviation was 0.487 t/ha as compared to 0.544 t/ha as the mean AGB and standard deviation of 0.09 t/ha estimated from UAV images. The mean AGB estimated from field inventory data in sample plot3 was 0.309 t/ha with the standard deviation of 0.426 t/ha while the mean AGB estimated from UAV images was 0.245 t/ha and the standard deviation was 0.221 t/ha.

Table 4.9: Estimated Biomass Descriptive Statistics

	Sample Plot1 Estimated Biomass(t/ha)		Sample Plot2 Estimated Biomass(t/ha)		Sample Plot3 Estimated Biomass(t/ha)	
	Field Biomass	UAV Biomass	Field Biomass	UAV Biomass	Field Biomass	UAV Biomass
Mean	0.576	0.613	0.622	0.546	0.309	0.245
Standard Error	0.089	0.007	0.099	0.018	0.053	0.027
Standard Deviation	0.704	0.057	0.487	0.090	0.426	0.221
Sample Variance	0.496	0.003	0.237	0.008	0.181	0.049
Total Biomass (t/ha)	36.269	38.604	14.93	13.123	20.092	15.932
Count	63	63	24	24	65	65
Confidence Level (95.0%)	0.177	0.014	0.205	0.038	0.106	0.054

Further comparison was performed where the paired two samples t- test for means was run to see if there were any notable differences between the mean tree AGB estimated from field inventory data and mean AGB estimated from UAV images (Table 4.10). The results show that there was no any significant difference between the mean tree AGB estimated from field inventory data and the mean tree AGB estimated from UAV images for t stat was less than the t critical two tail ($P>0.05$) in sample plot1. Likewise results presents no significant difference between the mean tree AGB estimated from field inventory data and the mean tree AGB estimated from UAV images as t stat < t critical two tail ($P>0.05$).

Table 4.10: t-Test - Sample plots Estimated Biomass Paired Two Sample for Means

	Sample plot1 Estimated Biomass		Sample plot2 Estimated Biomass		Sample plot3 Estimated Biomass	
	Field Biomass	UAV Biomass	Field Biomass	UAV Biomass	Field Biomass	UAV Biomass
t Stat	-0.475		0.765		1.072	
P(T<=t) one-tail	0.340		0.226		0.144	
t Critical one-tail	1.669		1.714		1.669	
P(T<=t) two-tail	0.679		0.452		0.287	
t Critical two-tail	2.0		2.008		1.998	

4.7.2 Biomass prediction Accuracy analysis

To assess the accuracy of the predicted biomass, RMSE for each sample plot was computed using equation 3.11 and the following results were achieved:

Sample plot1 $RMSE = \sqrt{\frac{1}{63}\sum_{i=1}^{63}(36.269 - 38.604)^2}$ = 0.087 t/ha

Sample plot2 $RMSE = \sqrt{\frac{1}{24}\sum_{i=1}^{24}(14.93 - 13.123)^2}$ = 0.015 t/ha

Sample plot3 $RMSE = \sqrt{\frac{1}{65}\sum_{i=1}^{65}(20.092 - 15.932)^2}$ = 0.516 t/ha

Furthermore, MPE for each sample plot were calculated using equation 3.12 where in sample plot1 the MPE was 0.099m while in sample plot2 MPE was -0.504m and in sample plot3 MPE was -0.318m

4.9 Overview of key findings

This study compared results of AGB estimated using UAV images to AGB estimated using field collected data which are treaded as the most accurate and therefore suitable for comparison (Salunkhe et al., 2018). Standard test methods were used where t-test results show that there is no significant difference between AGB estimated using both approaches.

Furthermore, the RMSE computed for each sample plot shows promising results for the method to be employed for AGB estimation.

CHAPTER FIVE

CONCLUSION AND RECOMMENDATIONS

5.1 Overview

This chapter gives a summary of the overall study findings in relation to research questions and finally gives some recommendations that may be adopted for future work to come up with the most realistic outcomes.

5.2 Conclusion

Many techniques for AGB estimation exist with varying degree of complexity in terms of data capture, processing and associated costs. This study used UAV images to estimate AGB of a small size urban forest as the simple and low-cost technique. The parameters extracted were used as inputs in the allometric models to estimate AGB. The technique was employed to assess if the extracted parameters can yield AGB similar to that estimated using field collected data.

The achieved results show that AGB estimated using UAV images has no significant difference from AGB estimated using data collected in the field, implying that Predicted DBH and tree heights extracted from UAV images well predicted AGB of the study area. This achieved small AGB discrepancy may be attributed to the fact that UAV images were timely taken in an off-leaf season that tree canopy obstruction for generation of accurate DEM was minimal.

UAV images were also assessed as to how they can produce reliable data for AGB estimation in small and medium size forests. The assessment was done by comparing the AGB estimated based on UAV images with AGB estimated based on field inventory data on each selected sample plot. The presented results with small significant difference suggest that UAV images can be effectively used for AGB estimations of small and medium size forests as can achieve reasonable accuracies.

5.3 Recommendations

Based on the study findings, the following recommendations are given

1) The use of UAV based techniques for management of forest resources should be encouraged down to local government authorities and individual companies in Tanzania as the simple and cost-effective technique for AGB estimation and collect other useful forest information that helps combat GHG in the atmosphere thence facilitate taking of appropriate measures to prevent much threats to climate patterns.

2) To diverse the choice of AGB estimation and results validation methods with increased possibility of extracting much forest parameters for future works, cameras capable of capturing information in red, green, blue and Infrared channels should be considered when taking the images.
3) To enhance the reliability of the DEM generated from UAV images, capturing of images should be done on an off- leaves season to overcome tree canopy cover obstructions.
4) More works are encouraged to establish AGB estimation models for urban forest

References

Agisoft. (2019). *Agisoft Metashape User Manual - Professional Edition, Version 1.5*. Retrieved on September 24, 2019 from https://www.agisoft.com/pdf/metashape-pro_1_5_en.pdf

Ali, Z., & Bhaskar, S. B. (2016). Basic statistical tools in research and data analysis. *Indian J Anaesth, 60*(9), 662-669. doi:10.4103/0019-5049.190623

Araya, M. M., & Hofstad, O. (2016). Monetary incentives to avoid deforestation Under REDD+. *Mitig Adapt Strateg Glob Change, 21*, 421–443. doi:10.1007/s11027-014-9607-y

Asier, R. L., & Lluis, B. (2019). Greenness Indices from a Low-Cost UAV Imagery as Tools for Monitoring Post-Fire Forest Recovery. *Drones, 3*(6). doi:10.3390/drones3010006

Avola, G., Gennaro, S. F. D., Cantini, C., Riggi, E., Muratore, F., Tornambè, C., & Matese, A. (2019). Remotely Sensed Vegetation Indices to Discriminate Field-Grown Olive Cultivars. *Remote Sensing, 11*(1242). doi:10.3390/rs11101242

Baatz, M., & Schäpe, A. (2000). Multiresolution Segmentation: an optimization approach for high quality multi-scale image segmentation. *In:Strobl,J., Blaschke, T. and Griesbner, G.,Eds., Angewandte Geographische Information-Verarbeitung, XII, Wichmann Verlag, Karlsruhe. Germany, 12-23.*

Batbaatar, A., Yongkai, L., Batbaatar, A., Chimidnyam, D., Fang., J., & Huifeng, H. (2019). Allometric Equations for Estimating the Above-Ground Biomass of Five Forest Tree Species in Khangai, Mongolia. *Forests, 10*(661). doi:10.3390/f10080661

Birdal, A. C., Avdan, U., & Türk, T. (2017). Estimating tree heights with images from an unmanned aerial vehicle. *Journal of Geomatics, Natural Hazards and Risk, 8*(2), 1144-1156. doi:10.1080/19475705.2017.1300608

Blozan, W. (2006). Tree measuring guidelines of the Eastern Native Tree Society. *Bulletin of the Eastern Native Tree Society., 1*(1).

Burgess, N. D., Bahane, B., Clairs, T., Danielsen, F., Dalsgaard, S., Funder, M., . . . Zahabu, E. (2010). Getting ready for REDD+ in Tanzania: a case study of progress and challenges. *Oryx, 44*(3), 339-351. doi:10.1017/s0030605310000554

Cerbu, G. A., Swallow, B. M., & Thompson, D. Y. (2011). Locating REDD: A global survey and analysis of REDD readiness and demonstration activities. *Environmental Science & Policy, 14*(2), 168-180. doi:10.1016/j.envsci.2010.09.007

Deng, S., Katoh, M., Guan, Q., Yin, N., & Li, M. (2014). Estimating Forest Aboveground Biomass by Combining ALOS PALSAR and WorldView-2 Data: A Case Study at Purple Mountain National Park, Nanjing, China. *Remote Sensing, 6*(9), 7878-7910. doi:10.3390/rs6097878

González-Jaramillo, V., Fries, A., Zeilinger, J., Homeier, J., Paladines-Benitez, J., & Bendix, J. (2018). Estimation of Above Ground Biomass in a Tropical Mountain Forest in Southern Ecuador Using Airborne LiDAR Data. *Remote Sensing, 10*(5). doi:10.3390/rs10050660

Guerra-Hernández, J., González-Ferreiro, E., Monleón, V., Faias, S., Tomé, M., & Díaz-Varela, R. (2017). Use of Multi-Temporal UAV-Derived Imagery for Estimating Individual Tree Growth in Pinus pinea Stands. *Forests, 8*(8). doi:10.3390/f8080300

Hiroyuki, M., Hibiki, M. N., Shin, N., Takeshi, M., Taku, M. S., Kenlo, N. N., & Nobuko, S. (2013). Spectral vegetation indices as the indicator of Photosynthesis. *Plant Ecology, 6*(5), 393–407. doi:10.1093/jpe/rts037

Holopainen, M., Vastaranta, M., & Hyyppä, J. (2014). Outlook for the Next Generation's Precision Forestry in Finland. *Forests, 5*(7), 1682-1694. doi:10.3390/f5071682

Ibrahim, E. M., & Osman, E. H. (2014). Diameter at Breast Height-Crown Width Prediction models for Anogeissus Leiocarpus (DC.) Guill &Perr and Combretum Hartmannianum Schweinf. *Journal of forest products & industries, 3*(4), 191-197.

Ibrahimi, E. (2018). Data analysis and documentation of statistics in biomedical research papers in Albania. *Biostatistics and Epidemiology International Journal, 2*(1).

Iizuka, K., Yonehara, T., Itoh, M., & Kosugi, Y. (2017). Estimating Tree Height and Diameter at Breast Height (DBH) from Digital Surface Models and Orthophotos Obtained with an Unmanned Aerial System for a Japanese Cypress (Chamaecyparis obtusa) Forest. *Remote Sensing, 10*(2). doi:10.3390/rs10010013

Jelle G, v. M., Bart, J. S., Eickhout., B., Rob, J. S., & Rik, L. (2008). Carbon Balance and Management. doi:10.1186/1750-0680-3-3

Jucker, T., Caspersen, J., Chave, J., Antin, C., Barbier, N., Bongers, F., . . . Coomes, D. A. (2017). Allometric equations for integrating remote sensing imagery into forest monitoring programmes. *Glob Chang Biol, 23*(1), 177-190. doi:10.1111/gcb.13388

Kachamba, D., Ørka, H., Gobakken, T., Eid, T., & Mwase, W. (2016). Biomass Estimation Using 3D Data from Unmanned Aerial Vehicle Imagery in a Tropical Woodland. *Remote Sensing, 8*(11). doi:10.3390/rs8110968

Kachamba, D., Ørka, H., Næsset, E., Eid, T., & Gobakken, T. (2017). Influence of Plot Size on Efficiency of Biomass Estimates in Inventories of Dry Tropical Forests Assisted by Photogrammetric Data from an Unmanned Aircraft System. *Remote Sensing, 9*(6). doi:10.3390/rs9060610

Lawrence, R. G. (1995). The Relationship of Diameter at Breast height and crown diameter. *Applied Forestry, 19*. https://doi.org/10.1093/sjaf/19.4.177

Lenda, G., Uznański, A., Strach, M., & Lewińska, P. (2016). Laser Scanning in Engineering Surveying: Methods of Measurement and Modeling of Structures. *Reports on Geodesy and Geoinformatics, 100*(1), 109-130. doi:10.1515/rgg-2016-0010

Li, D., Gu, X., Pang, Y., Chen, B., & Liu, L. (2018). Estimation of Forest Aboveground Biomass and Leaf Area Index Based on Digital Aerial Photograph Data in Northeast China. *Forests, 9*(275). doi:10.3390/f9050275

Lim, Y. S., ·La, P. H., ·Park, J. S., ·Lee, M. H., Pyeon, M. W., & ·Kim, J.-I. (2015). Calculation of Tree Height and Canopy Crown from Drone Images. *Korean Society of Surveying, Geodesy, Photogrammetry and Cartograph, 33*(6), 605-613. doi:10.7848/ksgpc.2015.33.6.605

Lu, D., Chen, Q., Wang, G., Moran, E., Batistella, M., Zhang, M., . . . Saah, D. (2012). Aboveground Forest Biomass Estimation with Landsat and LiDAR Data and Uncertainty Analysis of the Estimates. *International Journal of Forestry Research, 2012*, 1-16. doi:10.1155/2012/436537

Lu, D., Chen, Q., Wang, G., Moran, E., Batistella, M., Zhang, M., Saah, D. (2012). Aboveground Forest Biomass Estimation with Landsat and LiDAR Data and Uncertainty Analysis of the Estimates. *International Journal of Forestry Research, 2012*, 1-16. doi:10.1155/2012/436537

Macedo, F. L., Sousa, A. M. O., Gonçalves, A. C., Marques da Silva, J. R., Mesquita, P. A., & Rodrigues, R. A. F. (2018). Above-ground biomass estimation for Quercus rotundifolia using vegetation indices derived from high spatial resolution satellite images. *European Journal of Remote Sensing, 51*(1), 932-944. doi:10.1080/22797254.2018.1521250

Mahmut, D. A. (2004). The Relationships between Diameter at Breast Height, Tree Height and Crown Diameter in Calabrian Pines (Pinus brutia Ten.) of Baskonus Mountain, Kahramanmaras, Turkey. *Biological Sciences, 4*(4), 437-440.,doi: https://dx.doi.org/10.3923/jbs.2004.437.440

Malimbwi, R. E., Eid, T., & Chamshama, S. A. O. (2016). *Tree Biomass and Allometric Models in Tanzania*. Retrieved on January 18, 2020 from https://10.13140/RG.2.1.1891.5445

Malone, T., Liang, J., & Packee, E. C. (2009). *Cooperative Alaska Forest Inventory*. Retrieved January 20,2020 from https://doi.org/10.2737/PNW-GTR-785

Mauya, E. W., Mugasha, W. A., Njana, M. A., Zahabu, E., & Malimbwi, R. (2019). Carbon stocks for different land cover types in Mainland Tanzania. *Carbon Balance and Management, 14*(1). doi:10.1186/s13021-019-0120-1

Mugasha, W. A., Eid, T., Bollandsås, O. M., Malimbwi, R. E., Chamshama, S. A. O., Zahabu, E., & Katani, J. Z. (2012). *Allometric models for prediction of AGB for miombo woodlands in Tanzania*. Paper presented at the Proceedings of the first Climate Change Impacts, Mitigation and Adaptation Programme Scientific Conference.

Mugasha, W. A., Mwakalukwa, E. E., Luoga, E., Malimbwi, R. E., Zahabu, E., Silayo, D., . . . Kashindye, A. (2015). Allometric Models for Estimating Tree Volume and Aboveground Biomass in Lowland Forests of Tanzania. *International Journal of Forestry Research, 2016*. doi:10.1155/2016/8076271

Munishi, P. K. T., Mhagama, M., Muheto, R., & Andrew, S. M. (2008). The role of urban forestry in mitigating climate change and mitigation in Tanzania. *Tanzania Journal of Forestry and Nature Conservation, 77*. doi:10.4314/tjfnc.v77i1.40726

Murtiyoso, A., Grussenmeyer, P., Börlin, N., Vandermeerschen, J., & Freville, T. (2018). Open Source and Independent Methods for Bundle Adjustment Assessment in Close-Range UAV Photogrammetry. *Drones, 2*(1). doi:10.3390/drones2010003

Mutwiri, F. K., Odera, P. A., & Kinyanjui, M. J. (2017). Estimation of Tree Height and Forest Biomass Using Airborne LiDAR Data: A Case Study of Londiani Forest Block in the Mau Complex, Kenya. *Open Journal of Forestry, 07*(02), 255-269. doi:10.4236/ojf.2017.72016

NOAA. (2012). Lidar 101: An Introduction to Lidar Technology, Data, and Applications. In *Coastal Geospatial Services Division* (pp. 740-1200). 2234 S. Hobson Ave. Charleston, SC 29405 Coastal Services Center

Oniga, V.-E., Breaban, A.-I., & Statescu, F. (2018). Determining the Optimum Number of Ground Control Points for Obtaining High Precision Results Based on UAS Images. *Proceedings, 2*(7). doi:10.3390/ecrs-2-05165

Oppenheimer, M., & Petsonk, A. (2005). Article 2 of the UNFCCC: Historical Origins, Recent Interpretations. *Climatic Change, 73*(3), 195-226. doi:10.1007/s10584-005-0434-8

Ota, T., Ogawa, M., Shimizu, K., Kajisa, T., Mizoue, N., Yoshida, S., . . . Ket, N. (2015). Aboveground Biomass Estimation Using Structure from Motion Approach with Aerial Photographs in a Seasonal Tropical Forest. *Forests, 6*(12), 3882-3898. doi:10.3390/f6113882

Otero, V., Ruben, V. D. K., Behara, S., kolumba, M., Muhamad, A., Mohd Rodila, I., Farid, D.-G. (2018). Managing mangrove forests from the sky- Forest inventory using field data. *411*, 35-45. doi:http://doi.org/10.1016/j.foreco.2017.12.049

Özdemir, E., & Remondino, F. (2019). Classification of Aerial Point Clouds with deep learning. *The International Archives of the Photogrammetry, Remote Sensing and Spatial Information Sciences, XLII-2/W13*. doi:10.5194/isprs-archives-XLII-2-W13-103-2019

Penggang, J., Kai, X., Chen, D., Hailin, F., & Yinhui, Y. (2019). Predicting DBH of a single Ginkgo biloba tree based on UAV images. *36*(4), 757-763.

Pesso, G. G., Amorim, A., & Galo, M. (2018). Photogrammetric Point Cloud classification based on Geometric and Radiometric integration. *Bulletin of Geodetic Sciences, 25(spe)*(e2019s001). doi:10.1590/s1982-21702019000S00001

Puliti, S., Solberg, S., Næsset, E., Gobakken, T., Zahabu, E., Mauya, E., & Malimbwi, R. (2017). Modelling above Ground Biomass in Tanzanian Miombo Woodlands Using TanDEM-X WorldDEM and Field Data. *Journal of Remote Sensing, 9*(984). doi:10.3390/rs9100984

Salunkhe, O., Khare, P. K., Kumari, R., & Khan, M. L. (2018). A systematic review on the aboveground biomass and carbon stocks of Indian forest ecosystems. *Ecological Processes, 7*(1). doi:10.1186/s13717-018-0130-z

Schiewe., J. (2002). *Segmentation of high-resolution remotely sensed data - Concepts, Applications and Problems* Paper presented at the Symposium on Geospatial Theory, Processing and Applications, Ottawa Canada.

Schlund, M., & Davidson, M. (2018). Aboveground Forest Biomass Estimation Combining L- and P-Band SAR Acquisitions. *Remote Sensing, 10*(7). doi:10.3390/rs10071151

Schreyer, J., Geis, C., & Lakes, T. (2016). TanDEM-X for Large-Area Modeling of Urban Vegetation Height: Evidence from Berlin, Germany. *IEEE Journal of Selected Topics in Applied Earth Observations and Remote Sensing, 9*(5), 1876-1887. doi:10.1109/jstars.2015.2508660

Shi, L., & Liu, S. (2017). Methods of Estimating Forest Biomass- A Review. http://dx.doi.org/10.5772/65733.

Sileshi, G. W. (2014). A critical review of forest biomass estimation models, common mistakes and corrective measures. *Forest Ecology and Management, 329*, 237-254. doi:10.1016/j.foreco.2014.06.026

Sinha, S., Jeganathan, C., Sharma, L. K., & Nathawat, M. S. (2015). A review of radar remote sensing for biomass estimation. *International Journal of Environmental Science and Technology, 12*(5), 1779-1792. doi:10.1007/s13762-015-0750-0

Tang, L., & Shao, G. (2015). Drone remote sensing for forestry research and practices. *Journal of Forestry Research, 26*(4), 791-797. doi:10.1007/s11676-015-0088-y

Temesgen, H., Affleck, D., Poudel, K., Gray, A., & Sessions, J. (2015). A review of the challenges and opportunities in estimating above ground forest biomass using tree-level models. *Scandinavian Journal of Forest Research*, 1-10. doi:10.1080/02827581.2015.1012114

URT. (2017). *Tanzania's Forest Reference Emission Level Submission to the UNFCC*. Retrieved on February 3,2020 from https://redd.unfccc.int/files/frel__for__tanzania_december2016_27122016.pdf

Vashum, K. a. S. J. (2012). Methods to Estimate Above-Ground Biomass and Carbon Stock in Natural Forests - A Review. *Journal of Ecosystem & Ecography, 2*(4). doi:10.4172/2157-7625.1000116

Vazirabad, Y. F., & Karslioglu, M. O. (2011). Lidar for Biomass Estimation *Journal of Ecosystem & Ecography, 2*(116). doi:10.5772/16919

Wallace, L., Lucieer, A., Malenovský, Z., Turner, D., & Vopěnka, P. (2016a). Assessment of Forest Structure Using Two UAV Techniques: A Comparison of Airborne Laser Scanning and Structure from Motion (SfM) Point Clouds. *Journal of Forests, 7*(62). doi:10.3390/f7030062

Wallace, L., Lucieer, A., Malenovský, Z., Turner, D., & Vopěnka, P. (2016b). Assessment of Forest Structure Using Two UAV Techniques: A Comparison of Airborne Laser Scanning and Structure from Motion (SfM) Point Clouds. *Forests, 7*(12). doi:10.3390/f7030062

Watts, A. C., Ambrosia, V. G., & Hinkley, E. A. (2012). Unmanned Aircraft Systems in Remote Sensing and Scientific Research: Classification and Considerations of Use. *Remote Sensing, 4*(6), 1671-1692. doi:10.3390/rs4061671

Westoby, M. J., Brasington, J., Glasser, N. F., Hambrey, M. J., & Reynolds, J. M. (2012). 'Structure-from-Motion' photogrammetry: A low-cost, effective tool for geoscience applications. *Geomorphology, 179*, 300-314. doi:10.1016/j.geomorph.2012.08.021

Yavaşli, D. D. (2012). Recent approaches in AGB Estimation. *Aegean Geographical Journal, 21*(1), 39-51.

List of appendices

Appendix 1.1: Forest inventory data sheet

Msc Research- Forest Inventory - Ardhi University Neighbourhood Date--								
Tree ID	Sample Plot No	DBH(cm)	Desription	Sample Plot Corner X	Sample Plot Corner Y	Tree position X	Tree Position Y	Vertical Angle

Appendix 1.2: Level booking sheet

LEVEL SHEET							
Station	BS	IS	FS	HI	Corr	RL	Remarks

Appendix 1.3: List of Ground Control Points used for georeferencing

Point Id	Easting	Northing	Elevation	Description
CA09	523946.7877	9252343.791	39.461	GCP
CP3	523537.359	9252483.106	61.005	GCP
PT01	523891.1522	9251950.165	42.1083	GCP
PT02	523818.6954	9251937.886	45.9431	GCP
PT04	523939.2038	9252150.589	39.2962	GCP
PT11	523818.1794	9252243.017	44.051	GCP
PT13	523810.4429	9252285.412	44.0552	GCP
T1	523416.704	9252523.753	70.846	GCP
T4	523466.099	9252544.527	70.862	GCP
BB2	523910.394	9252342.549	40.7423	GCP
BB3	523914.9209	9252370.945	40.6253	GCP
BB4	523929.9049	9252368.244	40.389	GCP

Appendix 1.4: Calibration coefficients and correlation matrix

	Value	Error	F	Cx	Cy	B1	B2	K1	K2	K3	K4	P1	P2	P3	P4
F	7215.21	4.4	1.0	-0.06	-0.55	0.11	-0.11	0.13	-0.09	0.01	-0.03	0.12	-0.08	-0.09	0.07
Cx	25.5174	0.57		1.00	-0.08	0.28	0.58	-0.03	0.02	-0.02	0.02	0.42	-0.40	-0.32	0.23
Cy	33.2263	0.57			1.00	-0.54	0.16	-0.11	0.08	-0.04	0.05	-0.25	0.27	0.22	-0.18
B1	0.285819	0.57				1.00	0.09	0.07	-0.07	0.05	-0.05	0.04	-0.02	-0.06	0.02
B2	2.15507	0.057					1.00	-0.04	0.04	-0.04	0.04	0.05	-0.09	-0.04	-0.01
K1	0.0495893	0.00046						1.00	-0.97	0.92	-0.87	-0.01	0.03	0.03	-0.04
K2	-0.214471	0.0048							1.00	-0.98	0.96	0.03	-0.05	-0.06	0.08
K3	0.0787775	0.019								1.00	-0.99	-0.05	0.06	0.09	-0.10
K4	-0.129044	0.027									1.00	0.06	-0.07	-10	0.12
P1	0.000517933	2.6e-005										1.00	0.87	-0.94	0.88
P2	-0.00024958	1.3e-005											1.00	0.87	-0.81
P3	3.9415	0.46												1.00	-0.98
P4	-8.10909	0.91													1.00